arXiv:hep-ph/9601280v1 16 Jan 1996

CERN-TH/95-334
TAUP-2316-96
hep-ph/9601280

THE STRANGE SPIN OF THE NUCLEON[a]

JOHN ELLIS
Theory Division, CERN, CH-1211, Geneva 23, Switzerland,
e-mail: johne@cernvm.cern.ch

MAREK KARLINER
School of Physics and Astronomy,
Raymond and Beverly Sackler Faculty of Exact Sciences
Tel-Aviv University, 69978 Tel-Aviv, Israel
e-mail: marek@vm.tau.ac.il

The recent series of experiments on polarized lepton-nucleon scattering have provided a strange new twist in the story of the nucleon, some of whose aspects are reviewed in these lectures. In the first lecture, we review some issues arising in the analysis of the data on polarized structure functions, focusing in particular on the importance and treatment of high-order QCD perturbation theory. In the second lecture some possible interpretations of the "EMC spin effect" are reviewed, principally in the chiral soliton (Skyrmion) approach, but also interpretations related to the axial $U(1)$ anomaly. This lecture also discusses other indications from recent LEAR data for an $\bar{s}s$ component in the nucleon wave function, and discusses test of a model for this component. Finally, the third lecture reviews the implications of polarized structure functions measurements for experiments to search for cold dark matter particles, such as the lightest supersymmetric particle and the axion, after reviewing briefly the astrophysical and cosmological evidence for cold dark matter.

1 Polarized Structure Functions [b]

1.1 Formalism

The basis for our discussion will be the two spin-dependent structure functions G_1 and G_2:

$$\frac{d^2\sigma^{\uparrow\downarrow}}{dQ^2 d\nu} - \frac{d^2\sigma^{\uparrow\uparrow}}{dQ^2 d\nu} = \frac{4\pi\alpha^2}{Q^2 E^2}\left[M_N(E + E'\cos\theta)G_1(\nu, Q^2) - Q^2 G_2(\nu, Q^2)\right] \quad (1.1)$$

[a] Invited lectures at the Int. School of Nucleon Spin Structure, Erice, August 1995.
[b] This section is updated from Ref. [1].

In the parton model, these structure functions scale as follows in the Bjorken limit $x = Q^2/2M_N\nu$ fixed, $Q^2 \to \infty$:

$$\begin{aligned} M_N^2 \nu\, G_1(\nu, Q^2) &\equiv g_1(x, Q^2) \to g_1(x) \\ M_N \nu^2 G_2(\nu, Q^2) &\equiv g_2(x, Q^2) \to g_2(x) \end{aligned} \tag{1.2}$$

We will discuss the scaling structure function g_2 later on, focusing for now on g_1, which is related to the polarized quark distributions by

$$\begin{aligned} g_1^p(x) &= \frac{1}{2} \sum_q e_q^2 [q_\uparrow(x) - q_\downarrow(x) + \bar{q}_\uparrow(x) - \bar{q}_\downarrow(x)] \\ &= \frac{1}{2} \sum_q \Delta q(x) \end{aligned} \tag{1.3}$$

for comparison, the unpolarized structure function F_2 is given by

$$F_2(x) = \sum_q e_q^2 x [q_\uparrow(x) + q_\downarrow(x) + \bar{q}_\uparrow(x) - \bar{q}_\downarrow(x)] \tag{1.4}$$

so that the polarization asymmetry A_1 may be written as

$$A_1 = \frac{\sigma_{1/2} - \sigma_{3/2}}{\sigma_{1/2} + \sigma_{3/2}} \tag{1.5}$$

in the Bjorken limit, where $\sigma_{1/2}$ and $\sigma_{3/2}$ are the virtual photon absorption cross sections. We will discuss later the Q^2 dependences of the above formulae, as well as the transverse polarization asymmetry.

Much of the interest in the polarized structure function g_1 is due to its relation to axial current matrix elements:

$$\begin{aligned} \langle p | A_\mu^q | p \rangle &= \langle p | \bar{q} \gamma_\mu \gamma_5 q | p \rangle = \langle p | \bar{q}_R \gamma_\mu q_R - \bar{q}_L \gamma_\mu q_L | p \rangle = \\ &= \Delta q \cdot S_\mu(p) \end{aligned} \tag{1.6}$$

where $q_{L,R} \equiv 1/2(1 \mp \gamma_5)q$, S_μ is the nucleon spin four-vector, and

$$\Delta q \equiv \int_0^1 dx [q_\uparrow(x) - q_\downarrow(x) + \bar{q}_\uparrow(x) - \bar{q}_\downarrow(x)] \tag{1.7}$$

Of particular interest is the matrix element of the singlet axial current

$$A^0_\mu = \sum_{q=u,d,s} \bar{q}\gamma_\mu\gamma_5 q : \qquad \langle p|A^0_\mu|p\rangle = \sum_{q=u,d,s} \Delta q \cdot S_\mu(p) \tag{1.8}$$

which is related in the parton model to the sum of the light quark contributions to the proton spin. Prior to the series of measurements of polarized deep inelastic lepton nuclear scattering, information was available from charged current weak interactions on some axial current matrix elements. For example, neutron beta decay and strong isospin symmetry tell us that [2]

$$\Delta u - \Delta d = F + D = 1.2573 \pm 0.0028 \tag{1.9}$$

and hyperon beta decays and flavour $SU(3)$ symmetry tell us that [3]

$$\frac{\Delta u + \Delta u - 2\Delta s}{\sqrt{3}} \equiv \frac{a_8}{\sqrt{3}} = \frac{3F - D}{\sqrt{3}} = 0.34 \pm 0.02 \tag{1.10}$$

(for a recent discussion of the applicability of $SU(3)$ symmetry see Ref. [4] and references therein). Equations (1.9) and (1.10) give us two equations for the three unknowns Δu, Δd and Δs. In principle, a third piece of information was available [5,6] in 1987 from neutral current weak interactions. Measurements of νp and $\bar{\nu} p$ elastic scattering [7] indicated that

$$\Delta s = -0.15 \pm 0.09 \tag{1.11}$$

but this information was not generally appreciated before the advent of the EMC data discussed below. At present there is a new neutrino experiment under way at Los Alamos [8] which is expected to significantly improve the precision of (1.11) (see Ref. [9] for a recent in-depth analysis).

In the naive parton model, the integrals of the g_1 structure functions for the proton and neutron

$$\begin{aligned} \Gamma^p_1(Q^2) &\equiv \int_0^1 dx\ g^p_1(x, Q^2) \\ \Gamma^n_1(Q^2) &\equiv \int_0^1 dx\ g^n_1(x, Q^2) \end{aligned} \tag{1.12}$$

are related to combinations of the Δq.

$$\begin{aligned} \Gamma^p_1 &= \frac{1}{2}\left(\frac{4}{9}\Delta u + \frac{1}{9}\Delta d + \frac{1}{9}\Delta s\right) \\ \Gamma^p_1 &= \frac{1}{2}\left(\frac{1}{9}\Delta u + \frac{4}{9}\Delta d + \frac{1}{9}\Delta s\right) \end{aligned} \tag{1.13}$$

The difference between the proton and neutron integrals yields the celebrated Bjorken sum rule [10]

$$\Gamma_1^p(Q^2) - \Gamma_1^n(Q^2) = \frac{1}{6}(\Delta u - \Delta d) \times (1 - \alpha_s(Q^2)/\pi) + \ \ldots \tag{1.14}$$

It is not possible to derive individual sum rules for $\Gamma_1^{p,n}$ without supplementary assumptions. The assumption made by Ellis and Jaffe in 1973 [11] was that $\Delta s = 0$, on the grounds that very possibly there were a negligible number of strange quarks in the nucleon wave function, and if there were, surely they would not be polarized. With this assumption, it was estimated that

$$\begin{aligned} \int_0^1 dx g_1^p(x,Q^2) &= \frac{1}{18}(4\Delta u + \Delta d)\ (1 - \alpha_s/\pi + \ldots) = \\ &= 0.17 \pm 0.01 \end{aligned} \tag{1.15}$$

It should be clear that this was never a rigorous prediction, and was only intended as a qualitative indication to experimentalists of what they might find when they started to do polarized electron proton scattering experiments.

Perturbative QCD corrections to the above relations have been calculated [12–14] :

$$\begin{aligned} \int_0^1 [\, g_1^p(x,Q^2) - g_1^n(x,Q^2)\,] &= \frac{1}{6}\,|g_A|\, f(x) \ : \\ f(x) &= 1 - x - 3.58x^2 - 20.22x^3 + \ldots \end{aligned} \tag{1.16}$$

and

$$\begin{aligned} &\int_0^1 g_1^{p(n)}(x,Q^2) = \\ &= \left(\pm\frac{1}{12}\,|g_A| + \frac{1}{36}\,a_8\right)\, f(x) + \frac{1}{9}\,\Delta\Sigma(Q^2)\, h(x) \ : \\ &h(x) = 1 - x - 1.096x^2 - \ \ldots \end{aligned} \tag{1.17}$$

where $x = \alpha_s(Q^2)/\pi$, and the dots represent uncalculated higher orders of perturbation theory, to which must be added higher-twist corrections which we will discuss later. The coefficients in (1.16),(1.17) are for N_f=3, as relevant for the Q^2 range of current experiments.

With these corrections, the Bjorken sum rule is a fundamental prediction of QCD which can be used, for example, to estimate a value for $\alpha_s(Q^2)$. On the other hand, the individual proton and neutron integrals can be used to extract a value of Δs.

1.2 The Helen of spin

Early data on polarized electron-proton scattering from SLAC-Yale experiments [15,16,17] were compatible with the prediction of equation (1.15) within large errors. Over a 1000 theoretical and experimental papers were launched by the 1987 EMC result [18]

$$\int_0^1 g_1^p(x,Q^2) = 0.126 \pm 0.010 \text{ (syst.)} \ \pm 0.015 \text{ (stat.)} \quad , \\ \text{at } \langle Q^2 \rangle = 10.7 \text{ GeV}^2 \tag{1.18}$$

which was in *prima facie* disagreement with the dynamical assumption that $\Delta s = 0$. It is worth pointing out that the small-x behaviour of $g_1^p(x)$ was crucial to this conclusion. The earlier SLAC-Yale data had large extrapolation errors, and the EMC data indicated behaviour different from that in simple dynamical models. They were, however, consistent [5] with the naive Regge expectation [19]

$$g_1^p(x) \simeq \sum_i c_i \, x^{-\alpha_i(0)} \tag{1.19}$$

were the $\alpha_i(0)$ are the intercepts of axial vector Regge trajectories which are expected to lie between 0 and -0.5. A fit to the EMC data gave [5]

$$g_1^p \sim x^{-\delta} : \quad \delta = -0.07^{+0.42}_{-0.32} \ \text{ for } \ x < 0.2 \tag{1.20}$$

for $x < 0.2$.

Using equations (1.9),(1.10),(1.18) and the leading order perturbative QCD corrections in equation (1.17) it was estimated [20] that

$$\begin{aligned} \Delta u &= \ \ 0.78 \pm 0.06 \\ \Delta d &= -0.47 \pm 0.06 \\ \Delta s &= -0.19 \pm 0.06 \end{aligned} \tag{1.21}$$

Strikingly, these determinations corresponded to a total contribution of quarks to the proton spin

$$\Delta\Sigma = \Delta u + \Delta d + \Delta s = 0.12 \pm 0.17 \tag{1.22}$$

which was compatible with 0.

This has sometimes been called the "proton spin crisis", but we think this is an over-reaction. The result equation (1.22) was certainly a surprise for naive models of non- perturbative QCD, but it was not in conflict with perturbative QCD. Moreover, shortly after the first data became available it was shown [20] that $\Delta\Sigma = 0$ occurs naturally in the Skyrme model, which is believed to reproduce the essential features of QCD in the large-N_c limit. Alternatively, it was suggested that the $U(1)$ axial anomaly and polarized glue might provide an alternative interpretation [21–23], or a significant suppression of the QCD topological susceptibility [24–26] might play a key rôle, which would modify the naïve quark model predictions. These interpretations are discussed in more detail in Lecture II.

In 1972 Richard Feynman wrote "... *its [the Bjorken sum rule's] verification, or failure, would have a most decisive effect on the direction of future high-energy physics*". On the other hand, we think that the verification, or failure, of equation (1.22) has only an indecisive effect, though a very interesting one.

1.3 Evaluation of integrals

Before discussing the interpretation of more recent data on polarized structure functions, we first review a few points that arise in the evaluation of the integrals $\Gamma_1^{p,n}$. It should not be forgotten that the QCD versions of the sum rules are formulated at fixed Q^2. A generic deep-inelastic sum rule in QCD reads

$$\Gamma(Q^2) = \Gamma_\infty \left[1 + \sum_{n\geq 1} c_n \left(\frac{\alpha_s(Q^2)}{\pi} \right)^n \right] + \sum_{m\geq 1} \frac{d_m}{(Q^2)^m} \qquad (1.23)$$

where Γ_∞ is the asymptotic value of the sum rule for $Q^2 \to \infty$, the c_n are the coefficients of the perturbative corrections, and the d_m are coefficients of the so-called mass and higher-twist corrections. On the other hand, the data are normally obtained at values of Q^2 that increase on the average with x_{Bj} as seen in Fig. 1.1.

It is therefore necessary for each individual experiment to interpolate and extrapolate to some fixed mean value of Q^2, as indicated by the dashed horizontal line in Fig. 1.1. The quantity measured directly is the polarization asymmetry (1.5), which seems experimentally to have only small dependence on Q^2. In particular, a recent analysis by the E143 collaboration [27] sees no significant Q^2 dependence in A_1 for $Q^2 \gtrsim 1$ GeV^2, and the Q^2 dependence seen at lower Q^2 is compatible with the magnitude of the higher-twist correction

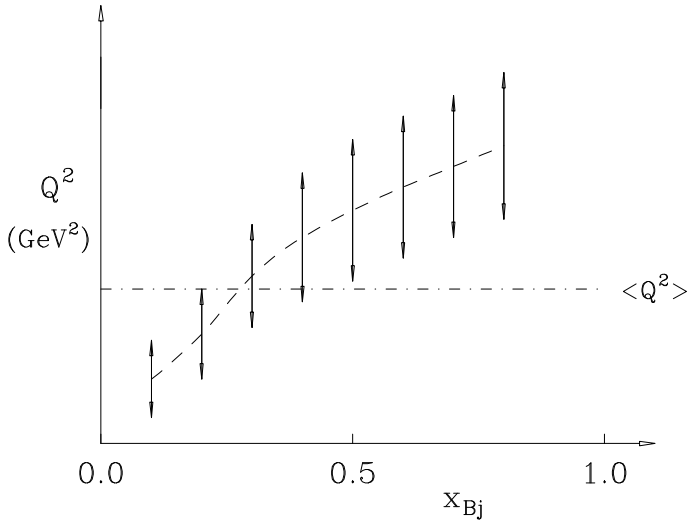

Figure 1.1: In any given polarized lepton-nucleon scattering experiment, the range of Q^2 probed is different in different bins of the Bjorken variable x_{B_j}.

discussed later. Therefore experiments often assume that A_1 is a function of x only, and then estimate

$$g_1(x,Q^2) = \frac{A_1(x,Q^2)F_2(x,Q^2)}{2x[1+R(x,Q^2)]} \simeq \frac{A_1(x)F_2(x,Q^2)}{2x[1+R(x,Q^2)]} \tag{1.24}$$

where $F_2(x,Q^2)$ and $R(x,Q^2)$ (the ratio of longitudinal to transverse virtual photon cross-sections) are taken from parametrizations of unpolarized scattering data. Note that these induce a Q^2 dependence in g_1 even if A_1 is independent of Q^2.

The possible reliability of the assumption that A_1 is independent of Q^2 can be explored using perturbative QCD models for $g_1(x,Q^2)$, and several such studies have been made [28–34]. Leading-order analyses indicated a small Q^2 dependence in $A_1(x,Q^2)$ (see eg. Ref. [28]), but higher-order analyses question this (see eg. Refs. [29], [34],[35]). The amount of any such Q^2 dependence is sensitive to the polarization of the gluon density $\Delta G(x,Q^2)$, and it may soon be possible to use data to constrain this, though we do not believe this is yet reliable [35] (see, however, Ref. [34]). It does not appear that such a Q^2 dependence in $g_1^{p,n}(x,Q^2)$ would have impact on the integrals $\Gamma_1^{p,n}(Q^2)$

outside the noted statistical and systematic errors. However, it could become an important effect in the future, and both theorists and experimentalists should keep their eyes open.

The old-fashioned assumption of Regge behaviour at low-x also needs to be checked carefully. The leading-order perturbative QCD evolution equations for the non-singlet part of the helicity distributions, $\Delta q_{NS}(x,Q^2)$, lead us to expect [36,37] singular behaviour as $x \to 0$, so that

$$\Delta q_{NS}(x,Q^2) \simeq C_{NS} \exp(A_{NS}\sigma + B_{NS}\frac{\sigma}{\rho} - \ln\rho - \frac{1}{2}\ln\sigma) \tag{1.25}$$

where A_{NS}, B_{NS} and C_{NS} are some constants and

$$\sigma \equiv \sqrt{\ln\frac{x_0}{x}\ln\frac{t}{t_0}}\,, \quad \rho \equiv \sqrt{\frac{\ln\frac{x_0}{x}}{\ln\frac{t}{t_0}}}\,, \quad t \equiv \left(\frac{\ln\frac{Q^2}{\Lambda^2}}{\ln\frac{Q_0^2}{\Lambda^2}}\right) \tag{1.26}$$

and we might expect by analogy with the unpolarized structure functions that $x_0 \sim 0.1$, $Q_0^2 \sim 1$ GeV and the leading-order QCD scale parameter $\Lambda \sim 0.25$ GeV, with

$$A_{NS} = \frac{4\sqrt{2}}{\sqrt{33-2N_f}}\,, \quad B_{NS} = \frac{4}{33-2N_f}\,. \tag{1.27}$$

where $N_f = 3$ in the Q^2 range of current experimental interest (see also Ref. [38]). In principle Eq. (1.25) can be applied directly to the low-x behavior of the integrand of the Bjorken sum rule: $g_1^p(x,Q^2) - g_1^n(x,Q^2) = \frac{1}{6}[\Delta u(x,Q^2) - \Delta d(x,Q^2)]$, as well as to the other nonsinglet combination $\Delta u(x,Q^2) + \Delta d(x,Q^2) - 2\Delta s(x,Q^2)$ that also contributes to $g_1^{p,n}(x,Q^2)$. The flavour-singlet combination of structure functions has a more complicated low-x behaviour, which could be important for the extraction of the Δq. It is not clear whether the behaviour in equation (1.25) is relevant to the data presently available: one SMC data point may be in its region of applicability, and could in principle be used to normalize the perturbative QCD formula, serving as a basis for extrapolating the integrals to $x = 0$. In practice, it does not seem at present that this would have a significant effect on the evaluation of the Bjorken sum rule.

The analysis of the polarized structure function data has often assumed that the transverse polarization asymmetry

$$A_\perp = \frac{d\sigma^{\downarrow\rightarrow} - d\sigma^{\uparrow\rightarrow}}{d\sigma^{\downarrow\rightarrow} + d\sigma^{\uparrow\rightarrow}}\,. \tag{1.28}$$

is negligible. This is related to the spin-flip photon absorption asymmetry

$$A_2 = \frac{2\sigma_{TL}}{\sigma_{1/2} + \sigma_{3/2}} \tag{1.29}$$

and the longitudinal A_1 asymmetry (1.5) through the relation:

$$A_\perp = d\,\left(A_2 - \gamma\,(1-\frac{y}{2})\,A_1\right)\,. \tag{1.30}$$

were $\sigma_{1/2}$ and $\sigma_{3/2}$ are the virtual photon–nucleon absorption cross sections for total helicity 1/2 and 3/2, respectively, σ_{TL} arises from the helicity spin-flip amplitude in forward photon–nucleon Compton scattering, $\gamma = 2Mx/\sqrt{Q^2}$, and $y = \nu/E_{lepton}$, where ν is the energy transfer in the laboratory frame. The coefficient d is related to the virtual photon depolarization factor D by

$$d = D\frac{\sqrt{1-y}}{1-y/2} \tag{1.31}$$

The asymmetries A_1 and A_2 are subject to the following positivity conditions[42]

$$|A_1| < 1\,, \qquad |A_2| \leq \sqrt{R}\,. \tag{1.32}$$

and are related to the structure functions $g_{1,2}$ by

$$A_1 = \frac{1}{F_1}(g_1 - \gamma^2 g_2)\,, \qquad A_2 = \frac{\gamma}{F_1}(g_1 + g_2)\,, \tag{1.33}$$

where $F_1 = F_2(1+\gamma^2)/2x(1+R)$ is the spin-independent structure function. Recently, data on g_2 have become available for the first time[43,44]. They indicate that it is considerably smaller than the positivity bound in equation (1.32), and is very close to the leading twist formula of Ref. [45]:

$$g_2^{\rm ww}(x,Q^2) = -g_1(x,Q^2) + \int_x^1 g_1(t,Q^2)\frac{dt}{t}\,, \tag{1.34}$$

The data on g_2 are also compatible with the Burkhardt-Cottingham sum rule [46]

$$\int_0^1 g_2(x,Q^2)dx = 0\,, \tag{1.35}$$

which has been verified to leading order in perturbative QCD[47,48]. The experimental errors are still considerable, in particular because the low-x behaviour of g_2 is less well understood than that of g_1. However, the data already tell us that the uncertainty in g_2 is not significant for the evaluations of the $\Gamma_1^{p,n}$.

1.4 Higher orders in QCD perturbation theory:

The perturbation series in QCD is expected to be asymptotic with rapidly growing coefficients:

$$S(x) = \sum_{n=0}^{\infty} c_n x^n \ , \quad x \equiv \frac{\alpha_s}{\pi} \ , c_n \simeq n! K^n n^\gamma \tag{1.36}$$

for some coefficients K, γ [49,50]. This type of behaviour is associated with the presence of the renormalon singularities, as we shall discuss shortly. Such series are often evaluated approximately by calculating up to the "optimal" order, implicitly defined by

$$|c_{n_{opt}} \, x^{n_{opt}}| < |c_{n_{opt}+1} \, x^{n_{opt}+1}| \tag{1.37}$$

and assuming an error of the same order of magnitude as $c_{n_{opt}} \, x^{n_{opt}}$. The question arises whether one can approach or even surpass this accuracy without calculating all the terms up to order n_{opt}. This possibility has been studied using the effective charge (ECH) approach [51,52] and using commensurate scale relations [53,54]. In this section, we discuss the use of Padé approximants (PA's) for this purpose [55,56].

Padé approximants [57,58] are rational functions chosen to equal the perturbative series to the order calculated:

$$\begin{aligned} [N/M] &= \frac{a_0 + a_1 x + ... + a_N x^N}{1 + b_1 x + ... + b_M x^M} \ : \\ [N/M] &= S + \mathcal{O}(x^{N+M+1}) \end{aligned} \tag{1.38}$$

Under certain circumstances, an expansion of the PA in equation (1.38) provides a good estimate, c^{est}_{N+M+1}, the Pade Approximant Prediction (PAP), for the next coefficient c_{N+M+1} in the perturbative series [59]. For example, we have demonstrated that if

$$\epsilon_n \equiv \frac{c_n \, c_{n+2}}{c^2_{n+1}} - 1 \ \simeq \ \frac{1}{n}, \tag{1.39}$$

as is the case for any series dominated by a finite number of renormalon singularities, then $\delta_{[N/M]}$ defined by

$$\delta_{[N/M]} \equiv \frac{c^{est.}_{N+M+1} - c_{N+M+1}}{c_{N+M+1}} \tag{1.40}$$

has the following asymptotic behaviour

$$\delta_{[N/M]} \simeq -\frac{M!}{L^M}\,, \qquad \text{where } L = N + M + a\,M \tag{1.41}$$

and where a is a number of order 1 that depends on the series under consideration. This prediction agrees very well with the known errors in the PAP's for the QCD vacuum polarization D function calculated in the large N_f approximation [60], as seen in Fig. 1.2a.

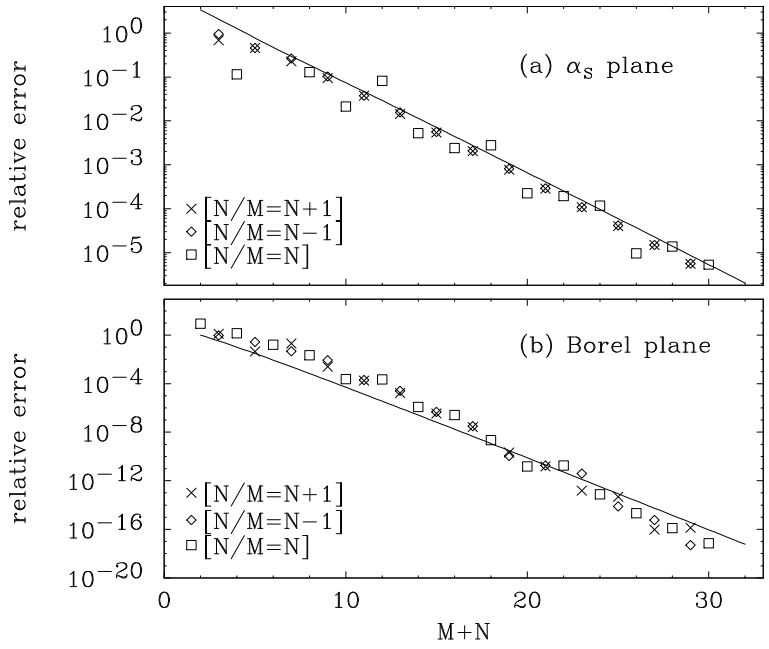

Figure 1.2: Relative errors in the $[N/M]$ Padé approximants (a) to the QCD vacuum polarization D-function, evaluated to all orders in the large-N_f approximation [60] (the rate of convergence agrees with expectations for a series with a discrete set of Borel poles), and (b) to the Borel transform of the D-function series, where the convergence is particularly striking. The straight lines correspond to the error formulae, eqs. (1.41) and (1.51), respectively.

Large-N_f calculations of the perturbative corrections to the Bjorken sum rule [61] indicate the presence of only a finite number of renormalon singularities, so that the PAP's should be accurate. Using the known terms in equation (1.16), the [1/2] and [2/1] PAP's yield the following estimates for the fourth-

order coefficient [56]:

$$\begin{aligned} c^{Bj}_{4[PA]} &\approx -111 \qquad ([1/2]\ \ \mathrm{PA}) \\ c^{Bj}_{4[PA]} &\approx -114 \qquad ([2/1]\ \ \mathrm{PA}) \end{aligned} \tag{1.42}$$

and the error estimator in equation (1.41) with $a = 1$ yields

$$\delta_{[1/2]} \simeq -1/8; \qquad \delta_{[2/1]} \simeq -1/4 \tag{1.43}$$

These results can be combined to obtain

$$c^{Bj}_{4[PA]} = \frac{1}{2}\left(\frac{-111}{1+\delta_{[1/2]}} + \frac{-114}{1+\delta_{[2/1]}} \right) \approx -139 \tag{1.44}$$

which is very close to the ECH estimate [52]

$$c^{Bj}_{4[ECH]} \simeq -130 \tag{1.45}$$

A second application of PA's is to "sum" the full perturbative series. The latter is ambiguous if the perturbative series possesses an infrared renormalon singularity, i.e. a divergence of the form in equation (1.36) with $K > 0$. Consider the following toy example:

$$\sum_0^\infty n!\, x^n = \int_0^\infty \frac{e^{-t}}{1-xt}\ dt = \frac{1}{x}\int_0^\infty \frac{e^{-y/x}}{1-y}\ dy \tag{1.46}$$

which exhibits an infrared renormalon pole at $y = 1$. One possible way to define the ambiguous integral on the right hand side of equation (1.46) is via the Cauchy principle value prescription [62]. We see in Fig. 1.3 that the errors in the Padé "Sums" (PS's) $[N/M](x)$ are smaller than the truncated perturbative series

$$\sum_{n=0}^{N+M} n!\, x^n \tag{1.47}$$

when $n < n_{opt}$, which is 5 in this example. You will notice in Fig. 1.3 that the errors in the PS's become unstable for large n: this is because of nearby poles in the denominator of equation (1.38) which are not important for small n. Also shown in Fig. 1.3 as "combined method" is a systematic approach to treating these poles and optimizing the PS's for large n, which is described elsewhere [63].

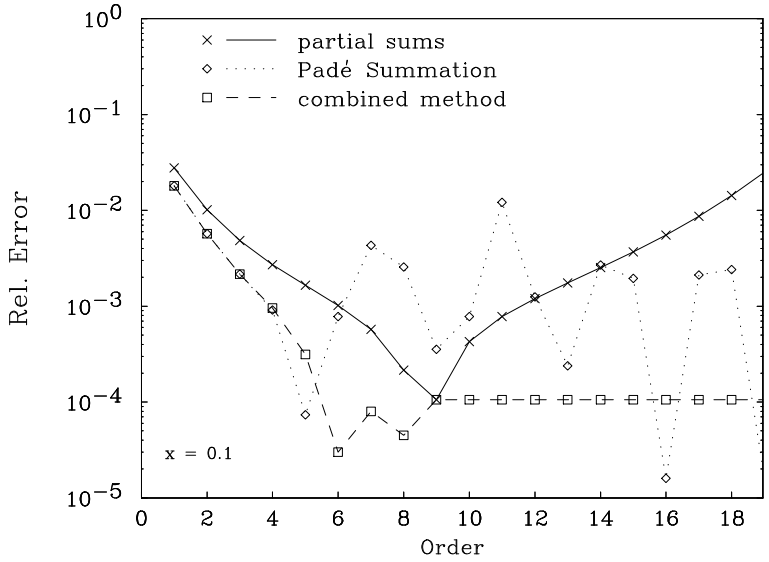

Figure 1.3: The relative errors between partial sums of the series $S(x) = \Sigma n! x^n$ and the Cauchy principal value of the series (solid line) is compared with the relative errors of Padé Sums (dotted line). We see that the relative errors of the Padé Sums are smaller than those of the partial sums in low orders, fluctuate in an intermediate régime, and are again more accurate than the partial sums in higher orders. The fluctuations are associated with nearby poles in the Padé Sums, that may be treated by the "combined method" mentioned in the text, shown as the dashed line.

Evidence that the PS's for the Bjorken sum rule provide a good estimate of the perturbative correction factor in equation (1.16) is provided by the study of the renormalization scale dependence. We see in Fig. 1.4 that the renormalization scale dependence of the [2/2] PS is much smaller than that of the [2/1] and [1/2] PS's, which is in turn much smaller than that of the naive perturbation series evaluated to third order. We recall[64] that the full correction factor should be scale-independent, and interpret Fig. 1.4 as indicating that the PS's may be very close to the true result.

Fig. 1.5 shows the estimates of the perturbative QCD correction to the Bjorken sum rule obtained in various different approximations, including third-order perturbation theory, fourth-order perturbation theory estimated using the ECH technique and the [2/1], [1/2] and [2/2] PS's. We interpret the latter as the best estimator, and take the difference between it and the [2/1] and [1/2] PS's as a theoretical uncertainty. Also shown in Fig. 1.5 is the experimental

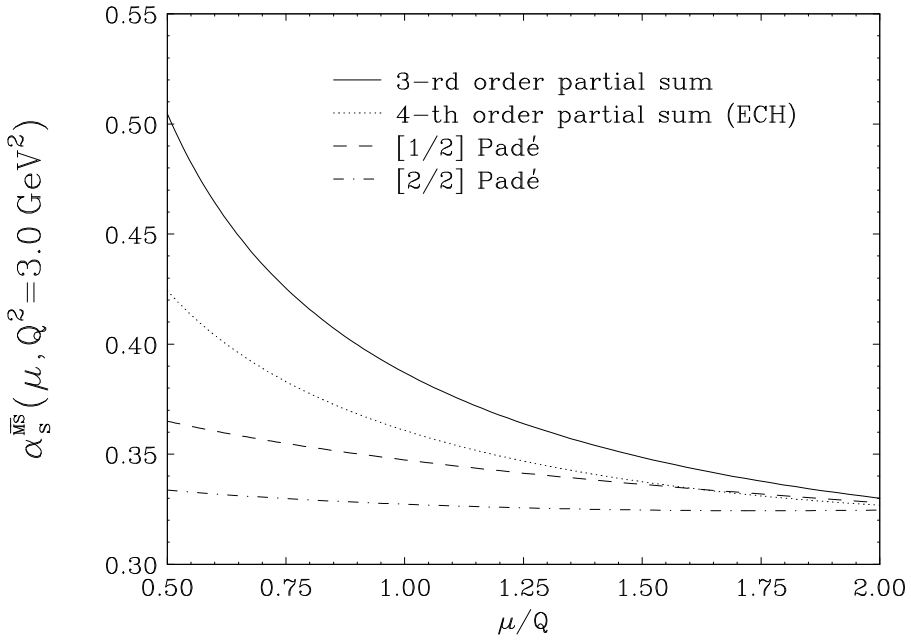

Figure 1.4: The scale dependence of $\alpha_s(3\mathrm{GeV}^2)$ obtained from a fixed value $f(x) = (6/g_A) \times 0.164 = 0.783$, (*cf.* eq. (1.54)), for $Q/2 < \mu < 2Q$, using the naive third- and fourth-order perturbative series and the [1/2] and [2/2] PS's.

error on this quantity, as extracted from the combined analysis of the available experimental data discussed in the next section.

More information can be extracted by considering PA's in the Borel plane. The Borel transform of a perturbative series is defined by

$$\begin{aligned} S(x) &= \sum_{n=0}^{\infty} c_n x^n \quad \underset{\text{Borel}}{\longrightarrow} \\ \tilde{S}(y) &\equiv \sum_{n=0}^{\infty} \tilde{c}_n y^n \;\; : \;\; \tilde{c}_n = \frac{c_{n+1}}{n!} \left(\frac{4}{\beta_0}\right)^{n+1} \end{aligned} \tag{1.48}$$

where $\beta_0 = (33 - 2N_f)/3$. A discrete set of renormalon singularities would show up as a set of finite-order poles in this plane

$$\frac{r_k}{(y - y_k)^P} \tag{1.49}$$

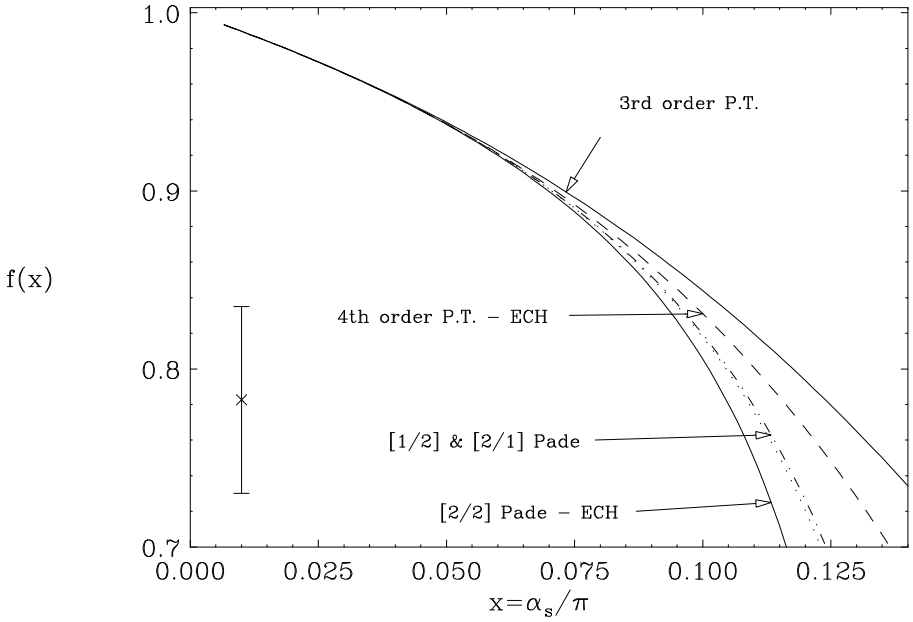

Figure 1.5: Different approximations to the Bjorken sum rule correction factor $f(x)$, third-order and fourth-order perturbation theory, [1/2], [2/1] and [2/2] Padé Sums are compared. Also shown as a vertical error bar is the value of $f(x)$ we extract from the available polarized structure data (1.54).

The PA's in equation (1.38) are clearly well suited to find the locations y_k and the residues r_k of such poles. In the case of a perturbative series dominated by a finite set of L renormalon singularities, a sufficiently high-order PA will be *exact*

$$[M/N](y) = \tilde{S}(y): \qquad \text{for } M+N > L_0 \tag{1.50}$$

for some $L_0 \propto L$. Generically, in any case where the quantity analogous to eq. (1.39), $\tilde{\epsilon}_n \simeq 1/n^2$, the error analogous to (1.40) is given by

$$\tilde{\delta}_{[M/M]} \simeq -\frac{(M!)^2}{L^{2M}} \tag{1.51}$$

This prediction of very rapid convergence is confirmed in Fig. 1.2b [55] in the case of the QCD vacuum polarization D function evaluated in the large N_f limit [60], which has an infinite number of renormalon poles.

The power of the application of PA's in the Borel plane is shown in Fig. 1.6, where we see that the [2/1] PA of the Borel-transformed Bjorken series has

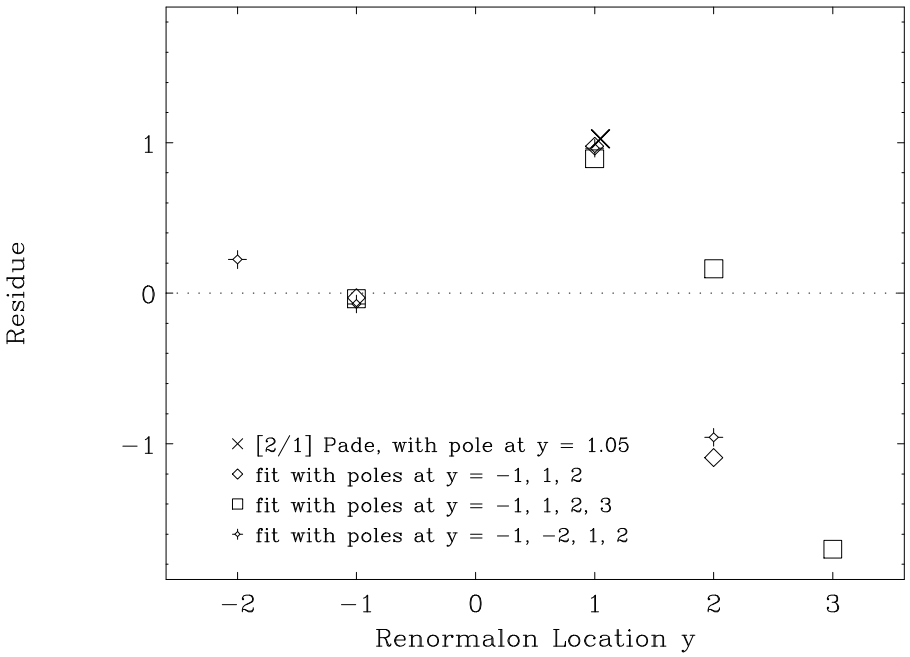

Figure 1.6: The locations and residues of poles in the [2/1] PA and in rational-function fits to the Borel transform of the first four terms in the perturbation series for the Bjorken sum rule. We note that the location of the lowest-lying infrared renormalon pole is estimated accurately by Padé Approximants in the Borel plane, and that its residue is stable in the different fits.

a pole at $y = 1.05$. The agreement with the expectation of a first infrared renormalon pole at $y = 1$ is striking. Fig. 1.6 also shows other rational-function approximations to the Borel-transformed Bjorken series. We see evidence that this is dominated by a strong infrared renormalon pole at $y = 1$, that there may be a weak ultraviolet renormalon pole at $y = -1$ and possibly another pole at $y = 2$.

The ambiguity in the definition of the perturbative Bjorken series associated with the $y = 1$ renormalon singularity corresponds to a possible $1/Q^2$ correction of magnitude [56]

$$\Delta\left(\Gamma_1^p - \Gamma_1^n\right) = \pm\frac{|g_A|}{6}\,0.98\,\pi\,\frac{\Lambda^2}{Q^2} \tag{1.52}$$

It is expected that the QCD correction to the Bjorken sum rule should include

a higher-twist correction of similar form with magnitude [65,66,67]

$$\Delta_{HT}\ (\Gamma_1^p - \Gamma_1^n) = -\frac{0.02 \pm 0.01}{Q^2} \tag{1.53}$$

The perturbative ambiguity in equation (1.52) is cancelled by a corresponding ambiguity in the definition of the higher-twist contribution. In the next section we will treat equation (1.53) as a correction (with error) to be applied to the perturbative QCD factor shown in Fig. 1.5.

We have also compared PA's to the predictions of commensurate scale relations within the framework of Ref. [54]. The predictions of the two approaches are numerically very similar, and we give formal reasons in Ref. [63] why we believe that this should be so. However, we shall not use commensurate scale relations in the data analysis of the next section.

1.5 Numerical analysis of the Bjorken sum rule

Table I shows the data on the integrals $\Gamma_1^{p,n}$ currently available from experiments at CERN and SLAC [18,68–70] . We do not attempt to correct these numbers for any of the effects discussed in section 1.4, such as the Q^2-dependence of the asymmetry A_1, the extrapolation to low-x, or the transverse polarization asymmetry. We do not believe that any of these effects will change any of the data outside their quoted errors. We choose to evaluate the Bjorken sum rule at $Q^2 = 3$ GeV^2, which requires rescaling all the data as described in Ref. [56].

Table I

$\Gamma_1^{p,n,d}$ currently available from experiments at CERN and SLAC.

experiment	target	Γ_1
E142	n	-0.045 ± 0.009
E143	p	0.124 ± 0.011
E143	d	0.041 ± 0.005
SMC	d	0.023 ± 0.025
SMC ('94)	d	0.030 ± 0.011
SMC	p	0.122 ± 0.016
EMC	p	0.112 ± 0.018

All experimental data have been evolved to $Q^2 = 3$ GeV^2.

The following is the combined result that we find for the Bjorken sum rule:

$$\Gamma_1^p(3\mathrm{GeV}^2) - \Gamma_1^n(3\mathrm{GeV}^2) = 0.164 \pm 0.011 \tag{1.54}$$

which is indicated by a vertical error bar in the lower left corner of Fig. 1.5. Comparing this value with the [2/2] PS estimate also shown there, we find

$$\alpha_s(3\ \mathrm{GeV}^2) = 0.328^{+0.026}_{-0.037} \tag{1.55}$$

which becomes

$$\alpha_s(M_Z^2) = 0.119^{+0.003}_{-0.005}\ \pm\ \ldots \qquad , \tag{1.56}$$

when we run α_s up to M_Z^2 using the three-loop renormalization group equation. The errors quoted in equations (1.55) and (1.56) are purely experimental, and the second $\pm$ sign in equation (1.56) indicates that further theoretical systematic errors must be estimated. Those we have evaluated include that associated with the renormalization scale dependence shown in Fig. 1.4 (± 0.002), the difference between the [2/2] and [2/1], [1/2] PS's (± 0.002), and the correction due to the higher-twist estimate in equation (1.53) (-0.003 ± 0.002), whereas the error in the running of α_s is found to be negligible. Combining these estimates with equation (1.56), we find [56]

$$\alpha_s(M_Z^2) = 0.116^{+0.003}_{-0.005} \pm 0.003\ , \tag{1.57}$$

The stability of this result is indicated in Fig. 1.7, where we exhibit the values of $\alpha_s(M_Z^2)$ obtained using different orders of perturbation theory, compared with our result (1.57) obtained using the [2/2] PS. Also indicated is the shift induced by the higher-twist correction, which lies within our error bars.

As can by seen from the compilation in Fig. 1.8, our central value for $\alpha_s(M_Z^2)$ is quite compatible with other determinations and the world average, which is quoted to be [2,71,72]

$$\alpha_s(M_Z^2) = 0.117 \pm 0.005 \tag{1.58}$$

Indeed, the error quoted in equation (1.57) is quite competitive with the most precise determinations of $\alpha_s(M_Z^2)$ that are available. Moreover, we note that plenty of precise new data will soon be available from the SMC experiment at CERN, the E154 and E155 experiments at SLAC, and the HERMES experiment [73] at DESY. In the longer run, experiments with a polarized proton beam at HERA will provide valuable information on the behaviour of g_1 at low-x, as well as on its Q^2-dependence at fixed x.

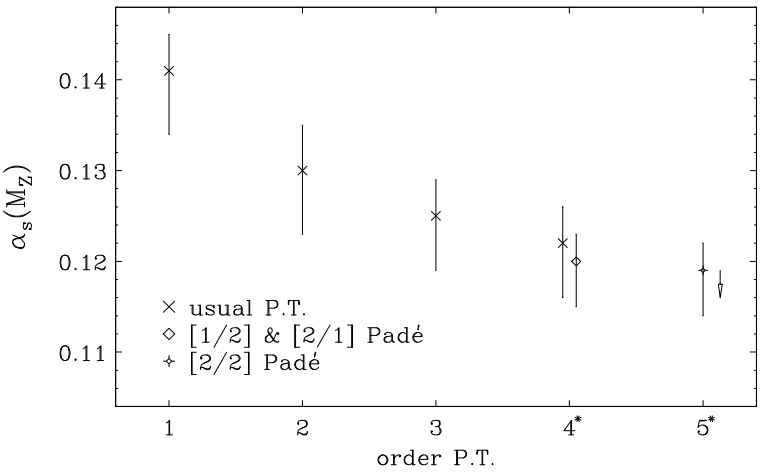

Figure 1.7: Values of $\alpha_s(M_Z^2)$ obtained using different orders of perturbation theory, compared with our result (1.56), obtained using the [2/2] PS. The size of the shift induced by higher-twist correction is (1.53) indicated by a downward arrow to the right of the [2/2] point.

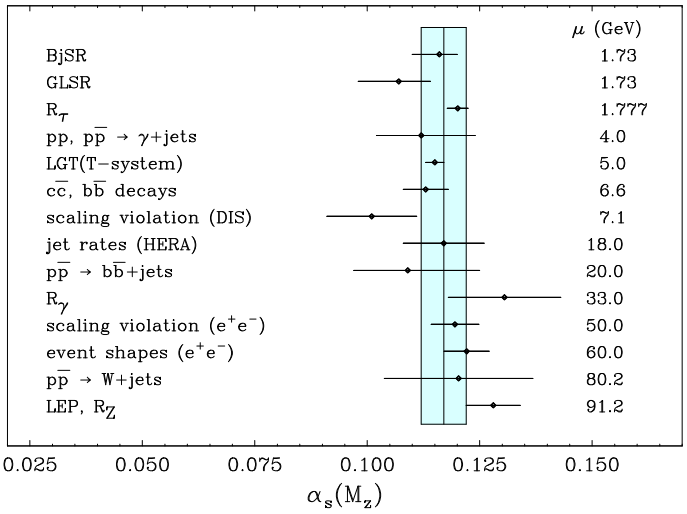

Figure 1.8: Compilation of world data on α_s from different sources (adapted from Ref. [72]).

1.6 Decomposition of the Nucleon Spin

So far, we have only discussed the combination $\Gamma_1^p - \Gamma_1^n$ which enters in the Bjorken sum rule. The individual $\Gamma_1^{p,n}$ can be used as in equation (1.13), though not forgetting the perturbative QCD corrections in equation (1.17), to extract the individual Δq. As is seen in Fig. 1.9, the different experiments on both proton and neutron targets are all highly consistent, *once the perturbative QCD corrections are taken into account.*

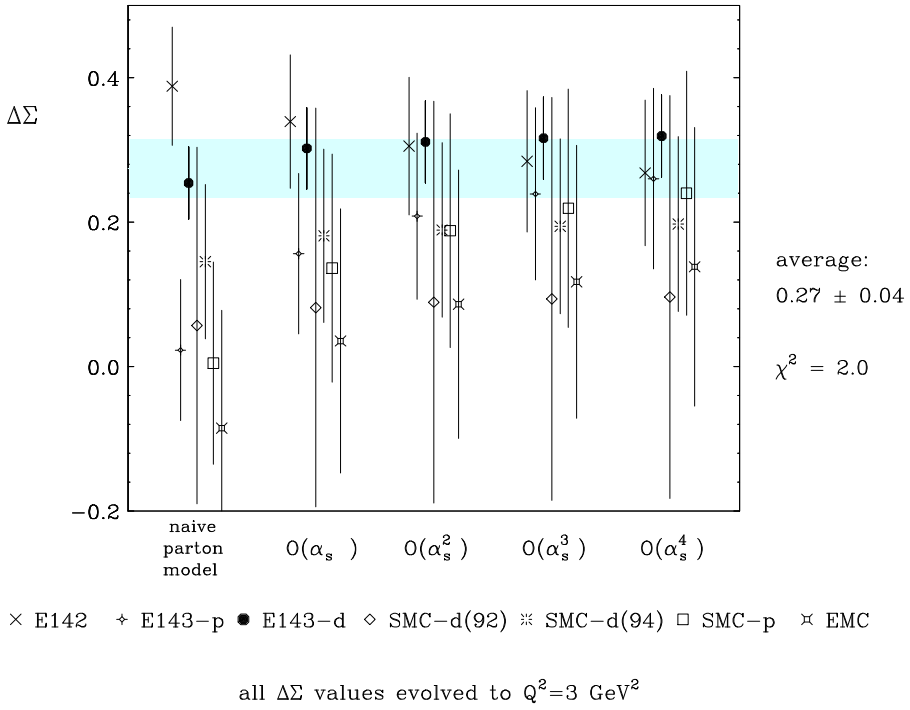

Figure 1.9: The values of $\Delta\Sigma(Q^2{=}3\ \mathrm{GeV}^2)$ extracted from each experiment, plotted as functions of the increasing order of QCD perturbation theory used in obtaining $\Delta\Sigma$ from the data (from Ref. [66], updated with most recent data).

Some time ago, it appeared as if the neutron data from E142 might be at variance with the other data points. However, this is no longer the case if all the higher-order corrections in equation (1.17) are taken into account, and the latest evaluations [70] of the E142 data indicate a different preliminary value of Γ_1^n, as seen in Table I. Making a global fit, we find

$$\begin{aligned} \Delta u &= 0.82 \pm 0.03 \pm \ldots \\ \Delta d &= -0.44 \pm 0.03 \pm \ldots \\ \Delta s &= -0.11 \pm 0.03 \pm \ldots \end{aligned} \tag{1.59}$$

and

$$\Delta\Sigma = \Delta u + \Delta d + \Delta s = 0.27 \pm 0.04 \pm \ldots \tag{1.60}$$

where the second $\pm$ sign indicates that further theoretical and systematic errors remain to be assigned. These include higher-twist effects, errors in the extrapolation to low-x which is more complicated than for the nonsinglet combination of structure functions appearing in the Bjorken integrand, the possible Q^2-dependence of A_1, etc.. We believe that these errors may combine to be comparable with the errors quoted in equations (1.59),(1.60), but prefer not to quote definitive ranges for the Δq until all these errors are controlled as well as those appearing in the Bjorken sum rule.

The SMC Collaboration has presented at this school a global analysis of the Δq [74], in which they combine SLAC and CERN measurements of the structure functions to arrive at new estimates of the $\Gamma_1^{p,n}$, which differ from the values we have used (see Table I) principally because of their treatment of the low-x data. An analysis of a subset of the the available data has also been presented in Ref. [34]. Both these analyses differ from ours in the treatment of higher-order perturbative QCD effects, but agree within the stated errors.

One may also get a feeling for the expected range of $\Delta\Sigma$ and Δs by plotting the results for these two observables extracted from each of the existing experiments, as shown in Fig. 1.10.

1.7 Outlook

In this lecture we have concentrated on the phenomenological analysis of the data on polarized structure functions presently available. As we have seen, these tell a remarkably consistent story, once higher-order QCD corrections are included. We have not addressed in great detail here the theoretical interpretation of the data, nor their spin-offs in hadron physics and elsewhere, nor possible future developments in this field. In fact, these measurements provide valuable insights into important issues in non-perturbative QCD, such as the role of chiral symmetry in nucleon structure [20], the axial anomaly and the $U(1)$ problem [21–26], and the relationship between current and constituent quarks [75–80] which are provoking lively theoretical debates (see Ref. [81] for a

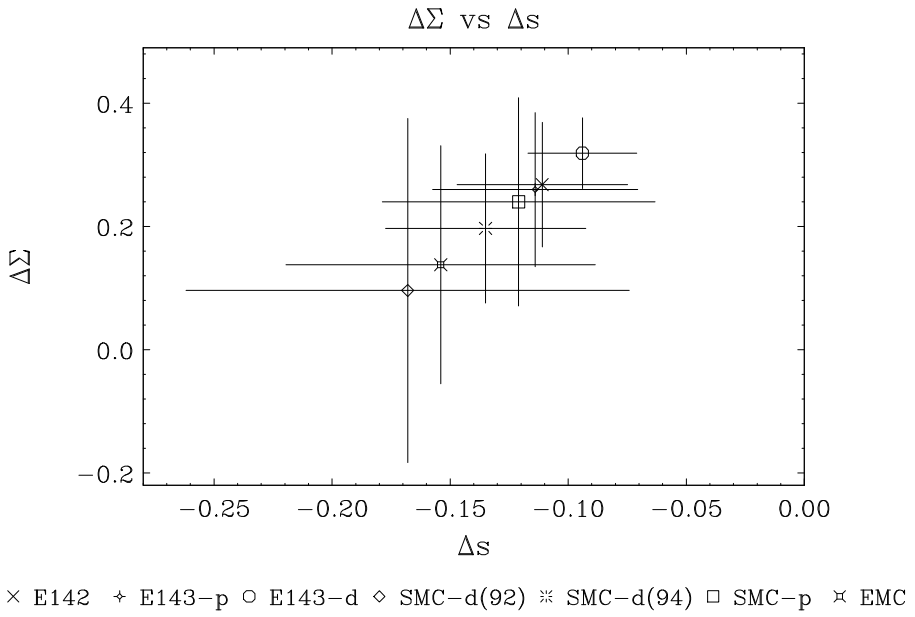

Figure 1.10: The values of $\Delta\Sigma$ and Δs extracted from each experiment, plotted against each other. All data have been evolved to common $Q^2 = 3$ GeV^2. The clear linear correlation between $\Delta\Sigma$ and Δs results from the linear relations (1.9),(1.10),(1.17).

recent application to the pion structure). Some of these issues are reviewed in Lecture II.

The polarized structure function data support previous indications from the π-nucleon σ-term and elsewhere that strange quarks in the nucleon wave function cannot be neglected, with interesting implications for the analysis of recent data from LEAR on ϕ production in proton-antiproton annihilation [82], as also discussed in Lecture II. Among other spin-offs, we recall that the axial-current matrix elements extracted from polarization data determine scattering matrix elements for candidate dark matter particles such as the lightest supersymmetric particle [83] and the axion [66], as discussed in Lecture III.

In the future, we look forward to the completion of the SMC programme and its possible HMC successor at CERN, the E154 and E155 experiments at SLAC, data from the HERMES experiment at HERA, the polarized proton programme at RHIC, and possible polarized electrons and protons in the HERA ring. The tasks of these experiments will include the determination

of the gluon contribution to the nucleon spin, the elucidation of the $Q,^2$ dependence of A_1, and the low-x behaviour of g_1. These will continue to fuel activity in this interesting field for the foreseeable future, which will lead us to a deeper understanding of the nucleon, an object we thought we knew so well, but which reveals a new face when it spins.

2 Chiral Solitons and Strangeness in the Nucleon

In this lecture, we review possible interpretations of the polarized structure function data, with particular emphasis on the chiral soliton (skyrmion) proposal [20], but with comments on other possibilities [21–26]. We also discuss indications from LEAR for a pattern of violations of the Okubo-Zweig-Iizuka (OZI) rule in ϕ production in $\bar{p}p$ annihilation, motivating a phenomenological model for $\bar{s}s$ component in the nucleon wave function, whose possible tests we also review.

2.1 Chiral soliton interpretation of EMC spin effect

In this section, we will describe a possible interpretation of EMC spin effect in terms of a chiral soliton model of hadrons. This has the double interest of being, as far as we know, the only model which *explains*[20] the small experimental value of $\Delta\Sigma$ and can also be derived from the underlying QCD theory, as we now describe (see Ref. [84] for a general introduction to QCD and its symmetries).

The classical QCD Lagrangian

$$\mathcal{L}_{QCD} = \mathcal{L}_{YM} - \sum_{q=1}^{N_f} (\bar{q}_L \not{D} q_L + \bar{q}_R \not{D} q_R) - \sum_{q=1}^{N_f} m_q (\bar{q}_L q_R + \bar{q}_R q_L) \tag{2.1}$$

is invariant under the following global chiral transformations

$$q_L \to L q_L \quad \text{and} \quad q_R \to R q_R; \quad L, R \in U(N_f) \tag{2.2}$$

which constitute the symmetry group $SU(N_f)_L \times SU(N_f)_R \times U(1)_V \times U(1)_A$, where $V = L + R$ and $A = R - L$. As will be discussed later, the $U(1)_A$ part of the chiral symmetry is broken by quantum effects, and we concentrate for now on the rest of the chiral symmetry group. It is believed that non-perturbative QCD dynamics break this chiral symmetry spontaneously to the subgroup $SU(N_f)_V$. In agreement with the Goldstone theorem, this spontaneous chiral symmetry breaking is accompanied by the appearance of $N_f^2 - 1$ Goldstone bosons, which are the $\pi^{\pm,0}$, $K^{\pm,0}$, $\bar{K}^0$, η_8 in the case of $SU(3)$ with the u, d, and s quarks. In the limit of small u, d, s quark masses, where $SU(3)_V$ symmetry becomes exact, the interactions of these light pseudo-scalar bosons are described by the following effective Lagrangian:

$$\begin{aligned} \mathcal{L}_{PS} &= \frac{f_\pi^2}{16} \mathrm{Tr}\left(\partial_\mu U \partial^\mu U^\dagger\right) + \frac{1}{32e^2} \mathrm{Tr}\left[(\partial_\mu U) U^\dagger, \partial^\mu U U^\dagger\right]^2 + \\ &+ \frac{f_\pi^2 m_{PS}^2}{8} \left(\mathrm{Tr}\, U - 2\right) + \mathcal{L}_{WZ} + \ldots \end{aligned} \tag{2.3}$$

where U is a matrix which represents the pseudoscalar Goldstone boson fields ϕ^a_{PS}, $a = 1 \ldots 8$:

$$U = \exp\left[\frac{2i}{f_\pi}\phi^a_{PS}\lambda_a\right] \tag{2.4}$$

The first term in (2.3) provides the P-wave $\pi\pi$ scattering lengths, as well as the canonical kinetic term for the boson fields. The second term contains higher order in the field derivatives, such as may be generated by vector-meson exchange, or by quark loops. The third term is related to the light quark masses, and yields

$$m^2_{PS} \propto \Lambda_{QCD}\, m_q\,. \tag{2.5}$$

When $N_f \geq 3$ there is an additional Wess-Zumino term $\mathcal{L}_{WZ}$ which does not concern us here.

The above effective Lagrangian (2.3) is believed to describe accurately QCD dynamics at energies $E \ll \Lambda_{QCD}$ for the light quarks [85]:

$$m_{u,d} \lesssim 10 \text{ MeV}, \qquad m_s \lesssim 150 \text{ MeV} \tag{2.6}$$

It may be regarded as the first step in a systematic bosonization of QCD, i.e., the expression of QCD dynamics in terms of meson fields. This bosonization can be derived formally in the $1/N_c$ expansion, which is often treated in the lowest-order approximation, though this is not necessary. In the $1/N_c$ expansion, one considers a replacement $SU(3)_c \to SU(N_c)$, in which

$$\alpha_s(Q^2) \simeq \frac{12\pi}{(11N_c - 2N_f)\,\ln Q^2/\Lambda^2} \tag{2.7}$$

We see explicitly that for large N_c the gauge coupling strength $g^2 \sim 1/N_c$. In

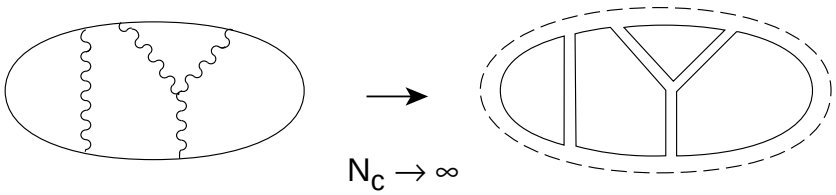

Figure 2.1: Planar diagrams for mesons in the large-N_c limit. The solid lines in the right-hand part represent colour lines, and the dashed line flavour.

this expansion, QCD is regarded as a theory of an infinite number of mesons, whose dynamics is described in leading order by planar diagrams such as those

in Fig. 2.1. It is easy to verify that these are all of the same order in the limit $N_c \to \infty$, $g^2 N_c$ fixed. Higher orders in the $1/N_c$ expansion may be treated systematically using diagrams of higher topological order. In two dimensions this programme has been realized explicitly; indeed QCD_2 has been "solved" for any value of N_c [86].

All well and good, but where are the baryons? The answer is that they are solitons in this apparently bosonic theory [87–93]. The energy of any field configuration described by the effective Lagrangian equation (2.3) can be written as

$$E = \int d^3\vec{x} \left\{ \frac{f_\pi^2}{16} \mathrm{Tr}\,(\vec{\partial} U \cdot \vec{\partial} U^\dagger) + \frac{1}{32e^2} \mathrm{Tr}\left[(\partial_i U) U^\dagger, (\partial_j U) U^\dagger \right]^2 + \ldots \right\} \tag{2.8}$$

This expression is finite if the following condition is satisfied:

$$U(\vec{x}) \to 1 \qquad \text{as} \qquad |\vec{x}| \to \infty \tag{2.9}$$

Elementary topology tells us that such field configurations are classified by the group $\Pi_3(SU(N_f)) = \mathbb{Z}$, which characterizes all the possible ways of mapping the 3-sphere into the chiral symmetry group. These different field configurations may be labeled by the quantity

$$B = \frac{1}{24\pi^2} \epsilon_{ijk} \int d^3\vec{x}\, \mathrm{Tr}\,(\partial_i U U^\dagger \partial_j U^\dagger \partial_k U U^\dagger) \tag{2.10}$$

which a topologist would identify as the winding number of the configuration. The quantity B is related in the normal way to a conserved current:

$$B = \int d^3\vec{x}\, J_0 \;\; : \quad \partial_\mu J^\mu = 0 \tag{2.11}$$

As discussed extensively elsewhere [89,90], B can be identified with baryon number. In the case of a spherically-symmetric soliton configuration:

$$U(\vec{x}) = \cos\theta(r) + i \frac{\vec{\tau} \cdot \vec{x}}{r} \sin\theta(r) \;\; : \quad r \equiv |\vec{x}| \tag{2.12}$$

one has:

$$B = \frac{1}{\pi} \left[\theta(0) - \theta(\infty) \right] \tag{2.13}$$

which is unity if $\theta(0) = \pi$ and $\theta(\infty) = 0$, which is the case for the lowest-energy soliton with $B = 1$. Also as discussed elsewhere [89,90] one can demonstrate that this $B = 1$ soliton is a fermion.

The above discussion may sound rather high-falutin', but the construction of such chiral solitons has been carried out explicitly in QCD in two dimensions [94] as we will discuss shortly.

An essential complication in the treatment of these chiral solitons is the fact that there are many equivalent soliton configurations: if U_0 is a solution, then so is

$$V_A \equiv V U_0 V^{-1} \tag{2.14}$$

where V is an arbitrary spatially-constant $SU(N_f)$ matrix. It is essential to take account of this when one quantizes the theory. This is done by parametrizing V in terms of its internal variables, the collective coordinates, and considering soliton wave functions $\chi(V)$ in the space of such collective coordinates:

$$|N\rangle = \int dV \chi(V) |V\rangle \tag{2.15}$$

At the quantum level, any state $|N\rangle$ must have definite isospin I and spin J,

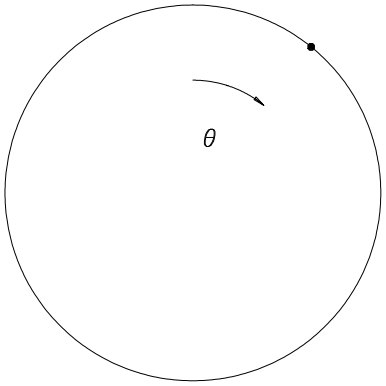

Figure 2.2: A one-dimensional analogue of the collective coordinate V: particle constrained to move on a circular ring. Classical ground state corresponds to a particle at rest at some fixed angle θ. In quantum mechanics this is no longer true and we must have an eigenstate of the angular momentum operator $L_\theta = -i\frac{\partial}{\partial\theta}$.

and this requires a superposition in the internal V space. The simplest way to see this is to consider the analogous case of a point particle located on a ring: $U_0 = e^{i\theta}$ in this case. Classically, the particle may sit at any fixed value of the angle θ. However, at the quantum level the only consistent state is an eigenstate of angular momentum, i.e., the point particle must rotate around the ring with an angular velocity ω, which is described by $V = e^{i\omega t}$! Exactly the

same phenomenon occurs with the $SU(N_f)$ chiral soliton: the quantum wave function must correspond to a rotation in the internal V space. This rotation ω is slow ($\sim 1/N_c$) in the large-N_c limit, in which a semi-classical treatment of the quantum state is sufficient, but one need not in principle restrict oneself to this assumption. In the limit of large N_c, the physical parameters of the soliton behave as follows [88,90] :

$$m_N \sim N_c\,, \quad R_N \sim N_c^0\,, \quad I \sim N_c\,, \quad J = \frac{1}{2} \sim N_c^0 \tag{2.16}$$

where R_N is the nucleon radius, and I its moment of inertia. The corresponding picture of the baryon that emerges is one of a rotating collective state of pseudoscalar mesons. The rotation velocity $\omega = J/I$ is slow in the limit of large N_c, but the underlying physical picture is valid in principle for any value on N_c.

As already mentioned, the above picture has been realized explicitly in QCD in two space-time dimensions for arbitrary values of N_c and N_f [94]. The solitons have precisely the form of equation (2.14), with the matrix U_0 taking the form

$$U_0 = \begin{pmatrix} 1 & & & & & \\ & 1 & & & & \\ & & . & & & \\ & & & . & & \\ & & & & . & \\ & & & & & \exp\, -i\sqrt{\frac{4\pi}{N_c}}\phi_0(x) \end{pmatrix} \tag{2.17}$$

where

$$\phi_0(x) = \sqrt{\frac{4N_c}{\pi}}\tan^{-1}\left[\exp\sqrt{\frac{8\pi}{N_c}}mx\right] \tag{2.18}$$

The $SU(N_f)$ rotation matrix V can be written in the form

$$V = \begin{pmatrix} & z_1 \\ & z_2 \\ \tilde{V} & . \\ & . \\ & . \\ & z_{N_f} \end{pmatrix} \tag{2.19}$$

where the form of $\tilde{V}$ does not concern us here, while the parameters $z_i : i = 1, \ldots, N_f$ play the role of the collective coordinates introduced earlier. They characterize the soliton solutions as follows:

$$\psi(z_i, z_j^*) = z_1^{n_1} \times z_2^{n_2} \times \ldots \times z_{N_f}^{n_{N_f}} \times z_1^{*m_1} \times \ldots z_{N_f}^{*\,m_{N_f}} \; : \sum_{i=1}^{N_f} (n_i - m_i) = N_c \tag{2.20}$$

The lowest-lying states lie in a **10** representation of $SU(3)$ analogous to that containing the Δ and Ω baryons in four dimensions. Thus we indeed have an explicit realization of the soliton ideas discussed previously. In particular, it is possible in this model to calculate the ratios of the matrix elements $\langle B|\bar{q}q|B\rangle$ in these baryon states [95]. In the general case of N_f flavors and N_c colors, one obtains

$$\langle (\bar{q}q)_{sea} \rangle_B = \frac{1}{N_f + N_c}, \tag{2.21}$$

where $(\bar{q}q)_{sea}$ refers to the non-valence quarks in the baryon B. One can also compute flavor content of valence quarks. Consider a baryon B containing k quarks of flavor v. The v-flavor content of such a baryon is

$$\langle \bar{v}v \rangle_B = \frac{k+1}{N_f + N_c} \tag{2.22}$$

For $N_f = 3$, $N_c = 3$ one finds

$$\begin{aligned} \langle \Delta^{++} | \bar{u}u \,,\, \bar{d}d \,,\, \bar{s}s | \Delta^{++} \rangle \;&\propto\; 4 \,,\, 1 \,,\, 1 \\ \langle \Omega^{-} | \bar{u}u \,,\, \bar{d}d \,,\, \bar{s}s | \Omega^{-} \rangle \;&\propto\; 1 \,,\, 1 \,,\, 4 \end{aligned} \tag{2.23}$$

We see explicitly that the $\bar{s}s$ matrix element in the non-strange baryon Δ^{++} is not negligible, and neither are the $\bar{u}u$, $\bar{d}d$ matrix elements in the triply-strange baryon Ω^-.

Unfortunately, it is not possible to explore axial-current matrix elements directly in this two-dimensional model, so we return to four dimensions.

In the picture of spontaneously-broken chiral symmetry, the matrix elements of axial currents are given in general by the PCAC hypothesis, namely that they are dominated by couplings of the pseudoscalar Goldstone boson with the same quantum numbers. We know from $\pi^\pm$ decay that

$$\langle 0 | A_\mu | \pi \rangle = i f_\pi p_\mu \tag{2.24}$$

and similarly for the $K^{\pm}$, and the same is believed to be true for other members of the pseudoscalar-meson octet. Matrix elements of the $SU(3)$ octet axial currents are related to the couplings of the octet pseudoscalars:

$$\langle X|A^i|Y\rangle \propto f_\pi g_{\phi^i_{PS}XY} \,. \tag{2.25}$$

The ninth axial current is special, because it is not conserved at the quantum level [96]:

$$\partial^\mu A^0_\mu \;\propto\; g^2 F_{\mu\nu}\tilde{F}^{\mu\nu} \tag{2.26}$$

For this reason, the ninth pseudoscalar η^0 is only a pseudo-Goldstone boson, whose mass would be non-zero even if $m_{u,d,s} = 0$ [97] :

$$m_{\eta_0} \;\propto\; 1/N_c \tag{2.27}$$

It should also be noted that the ninth pseudoscalar decouples from the other eight in the limit of large N_c since its couplings to them proceed via intermediate gluons [85] : for example, there is a coupling

$$\mathcal{L}_{\pi,\eta_0} = \frac{f_\pi^2}{16}\,\mathrm{Tr}\,(\partial_\mu U \partial^\mu U^\dagger)\frac{\eta_0^2}{N_c^2} \tag{2.28}$$

As already commented, the chiral soliton exists because of the topology of $SU(N_f)$, not that of $U(1)$. This means that the baryon is to be regarded as a "lump" of the $\pi/K/\eta_8$ mesons, *not* the singlet η_0. Moreover, equation (2.28) indicates that the η_0 decouples from the baryon at leading order in $1/N_c$.

Chiral soliton calculations are generally made in the relatively easy limits $N_c \to \infty$, $m_{u,d,s} \to 0$. One should beware of N_c-dependent predictions, which depend on the truncation of the *a priori* infinite-dimensional meson theory. Examples of such bad N_c-dependent quantities include

$$\mu_p \,,\; \mu_n \,,\; g_A \,,\; f_\pi \,,\; g_{\pi NN} \,,\; g_{\pi N\Delta} \,, \ldots \tag{2.29}$$

On the other hand, calculations of N_c-independent quantities such as

$$\begin{array}{cccc} \langle r^2\rangle_N \,, & \mu_p/\mu_n \,, & f_\pi^2/g_A \,, & g_{\pi N\Delta}/g_{\pi NN} \\ (19\%) & (2\%) & (3\%) & (1\%) \end{array} \tag{2.30}$$

may not be so unreliable, as indicated by the accuracy of the predictions listed above [98]. Another example of a quantity which may be reliably estimated in the $SU(3)_f$ limit is [99]

$$\frac{\langle p|\bar{s}s|p\rangle}{\langle p|\bar{u}u + \bar{d}d + \bar{s}s|p\rangle} = \frac{7}{30} \tag{2.31}$$

and this number is indeed consistent with determinations of the π-nucleon σ term. The chiral soliton model has also demonstrated successes in calculations of meson-baryon scattering phase shifts [100,101].

The chiral soliton model offers three ways of seeing that $\langle p|A^0_\mu|p\rangle \simeq 0$, i.e. that $\Delta u + \Delta d + \Delta s \simeq 0$ [20]. The brute-force method is by direct calculation using the following standard representation of $A^i_a(x)$ in the soliton state

$$\int d^3\vec{x}\, A^i_a(\vec{x}) \;\propto\; \mathrm{Tr}\left[\lambda_a V^{-1}\lambda_i V\right] \tag{2.32}$$

it is easy to see that the matrix element of A^0_a vanishes because $\mathrm{Tr}(\lambda_a) = 0$.

The second way to see the vanishing of $\langle p|A^0_\mu|p\rangle$ is to consider the Goldberger-Treiman relation for the baryonic matrix element of the ninth axial current. As discussed above, the PCAC hypothesis relates this to the baryonic coupling of the ninth pseudoscalar meson η_0. To see that this coupling vanishes, it suffices to make another trivial trace over $SU(N_f)$ indices:

$$g_{\eta_0 NN} \;\propto\; \mathrm{Tr}\left(\lambda_i \hat{U}(\vec{x})\right) = \mathrm{Tr}\left(\lambda_i V \hat{U}_0 V^{-1}\right) \tag{2.33}$$

This vanishing result can be understood at a more basic level by remembering that the baryonic soliton consists of π, K and η_8 mesons alone in the large-N_c limit, and that the η_0 meson decouples from the others in this same limit.

The third way of seeing that $\langle p|A^0_\mu|p\rangle \simeq 0$ is to consider the underlying physics of the soliton spin, by analogy with the particle on a ring discussed earlier. At the classical level, the baryon mass is given simply by

$$M = \int d^3\vec{x}\, \Theta_{00}(\vec{x}) \tag{2.34}$$

where the energy-momentum tensor $\Theta_{\mu\mu}$ is derived from a static solution $U_0(x)$. However, we recall that this is not an eigenstate of spin or isospin: these rotate with an angular velocity $\omega \sim 1/N_c$. The resulting expression for the soliton angular momentum is

$$J_i = \int d^3\vec{x}\, \epsilon_{ijk} x_j\, \Theta_{0k}(\vec{x}) = \omega_i\, I \tag{2.35}$$

where

$$I = \frac{2}{3}\int d^3\vec{x}\, \Theta_{00}\, r^2 \tag{2.36}$$

is its moment of inertia. Including the corresponding rotational energy, equation (2.34) is modified to become

$$M = \int d^3\vec{x}\, \Theta_{00}(\vec{x}) + \frac{J(J+1)}{2I} \tag{2.37}$$

where the quantization of angular momentum imposes

$$J(J+1) = \frac{3}{4} \text{ for } N, \quad \frac{15}{4} \text{ for } \Delta \tag{2.38}$$

We see explicitly from this construction that *all* the nucleon angular momentum is orbital in origin. If we consider the angular momentum sum rule

$$\frac{1}{2} = \frac{1}{2}\sum_q \Delta q + \Delta G + L_z \tag{2.39}$$

this argument tells us that

$$\Delta\Sigma = \sum_q \Delta q = 0, \qquad L_z = \frac{1}{2} \tag{2.40}$$

Simple models which extend the chiral soliton model to include gluons suggest also that [5]

$$\Delta G = 0 \tag{2.41}$$

These results have been derived in the limit of large N_c and small $m_{u,d,s}$. Attempts have been made to calculate corrections to this double limit, but these are incomplete so far. Nevertheless, naïve guess and incomplete calculations suggest that the result equation (2.40) might be accurate to within 30% or so. Since this range includes the present experimental value discussed in Lecture I, we consider this an encouraging success for the chiral soliton model.

An alternative approach [21–23] to interpreting the polarized structure function data is based on the axial $U(1)$ anomaly, which should be taken into account in computing matrix elements of the singlet axial current. The definition of the polarized quark distribution $\Delta q(x, Q^2)$ is ambiguous at the 1-loop level. One possible interpretation replaces

$$\Delta q \to \widetilde{\Delta q} \equiv \Delta q - \frac{\alpha_s}{2\pi}\Delta G \tag{2.42}$$

where the second term on the right-hand side is derived from the gluon contribution ΔG to the proton spin. In this interpretation all the previous determinations of Δq should be rephrased as determinations of the $\widetilde{\Delta q}$, and it is possible, in principle, to resurrect the original quark model assumption by postulating that

$$\widetilde{\Delta s} = \Delta s - \frac{\alpha_s}{2\pi}\Delta G \neq 0 : \qquad \Delta s = 0,\ \Delta G \neq 0 \tag{2.43}$$

In order for this mechanism to work, the value of ΔG must be quite large

$$\Delta G \simeq 2 \tag{2.44}$$

at $Q^2 \simeq 3$ GeV^2. This requires what might at first sight appear to be a rather bizarre decomposition of the proton angular momentum:

$$\frac{1}{2} \simeq \frac{1}{2} + (\simeq 2) + (\simeq -2) \tag{2.45}$$

However, it should be noted that a leading-order compensation between large values of ΔG and L_z is natural in perturbative QCD. Nevertheless, this anomalous gluon mechanism does not really explain the EMC result, though it may accommodate it. It is not yet possible to test definitively this model. For one thing, the x-dependence of the possible ΔG contribution requires further specification. So far we are aware of just one experimental result which bears on ΔG: a Fermilab fixed-target experiment has searched for an asymmetry in multiple γ production in polarized proton-proton collisions [103].

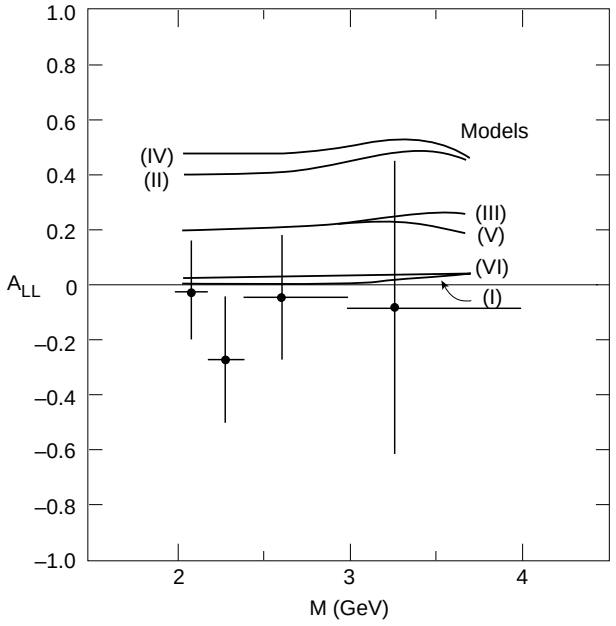

Figure 2.3: The particle production asymmetry A_{LL} measured in Ref. [103], compared with various phenomenological models labeled by the curves (I) to (VI), as functions of the effective mass M of the produced system.

As seen in Fig. 2.3, they see no significant asymmetry, which is in conflict with some polarized-gluon models, but not all [104]. Unravelling the polarization of the gluons in the proton is one of the primary objectives of the next round of polarization experiments such as the HMC and RHIC.

In addition to the soliton and anomaly interpretation, it was also suggested [24–26] that a significant suppression of the QCD topological susceptibility might play a key rôle, which would modify the naïve quark model predictions (see also the discussion in Lecture I).

2.2 The Okubo-Zweig-Iizuka Rule

The polarized structure function experiments are not alone in indicating that there may be strange quarks inside the proton wave function. Other indications come from experimental violations of the Okubo-Zweig-Iizuka (OZI) rule [105], as discussed in the rest of this lecture.

According to the OZI rule, the only strong-interaction processes allowed are those which can proceed via connected quark line diagrammes such as those shown in Fig. 2.4.

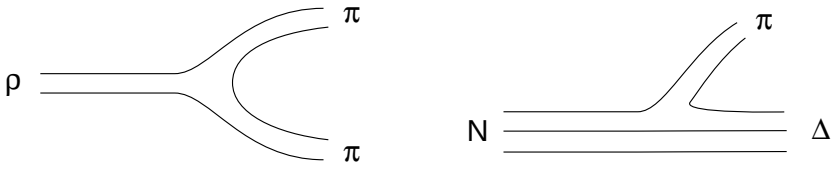

Figure 2.4: Connected quark line diagrams for ρ decay and the $\pi n \Delta$ coupling, using the naive quark model content of the particles, and hence corresponding to processes conventionally allowed by the OZI rule.

This assumption must be supplemented by Ansätze for hadron wave functions, such as the naïve quark model contents

$$|\phi\rangle = |\bar{s}s\rangle\,, \quad |p\rangle = |uud\rangle \tag{2.46}$$

Indications from meson mass formulae and the observation of $\phi \to 3\pi$ decay are that the ϕ wave function is actually a mixture:

$$|\phi\rangle = \cos\,\delta\,|\bar{s}s\rangle\, +\, \sin\,\delta\,|\bar{u}u\, +\, \bar{d}d\,\rangle/\sqrt{2} \tag{2.47}$$

where $\delta \ll 1$. Disconnected diagrams may be mediated by gluon exchange, as

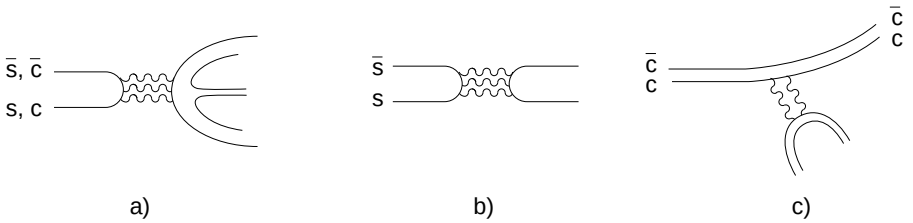

Figure 2.5: Disconnected diagrams mediated by gluon exchange, relevant to (a) ϕ and J/ψ decays, (b) a departure from ideal mixing in the ϕ wave function, and (c) transitions between different charmonium states.

shown in Fig. 2.5, which are subject to dynamical suppression which depends on the process considered:

$$\frac{g^2_{\phi 3\pi}}{g^2_{\omega 3\pi}} \sim 10^{-2}\,, \quad \frac{g^2_{f'\pi\pi}}{g^2_{f\pi\pi}} \sim 10^{-3}\,, \quad \frac{\Gamma_{J/\psi}}{\Gamma_{had}} \sim 10^{-4}\,, \quad \frac{\Gamma_{J/\psi\pi\pi}}{\Gamma_{had}} \sim 10^{-2} \tag{2.48}$$

The OZI rule finds some justification in the large-N_c limit of QCD considered earlier. Simple N_c power-counting for the meson diagrams in Fig. 2.6 shows that they are suppressed by $1/N_c$ and $1/N_c^2$, respectively.

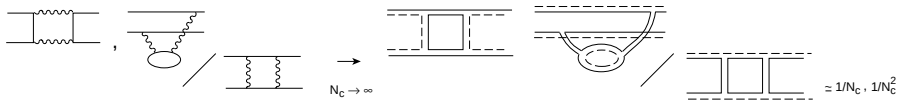

Figure 2.6: Meson diagrams that are suppressed in the large-N_c limit. As in Fig. 2.1, the solid lines represent colour, and the dashed lines flavour.

However, the applicability of the OZI rule to baryons is more questionable [102]. It is more difficult to justify in the large N_c limit, because the baryon wave function contains $\mathcal{O}(N_c)$ quarks. Moreover, it does not seem to work very well experimentally. Historically, one of the first indications of a discrepancy with the OZI rule was the π-nucleon σ-term [106,107] :

$$\Sigma^{\pi N} = \frac{1}{2}(m_u + m_d)\langle p|\bar{u}u + \bar{d}d|p\rangle \tag{2.49}$$

Using the Gell-Mann-Okubo mass formula and the OZI assumption that $\langle p|\bar{s}s|p\rangle = 0$ one estimates

$$\Sigma^{\pi N} \simeq 25 \text{ MeV} \tag{2.50}$$

to be compared with the experimental value of about 45 MeV, corresponding to

$$\frac{\langle p|\bar{s}s|p\rangle}{\langle p|\bar{u}u+\bar{d}d+\bar{s}s|p\rangle} \simeq 0.2 \tag{2.51}$$

The data on polarized structure functions discussed in Lecture I provide another example of an $\bar{s}s$ matrix element in the proton which is non-negligible.

In addition to these static matrix elements, there have long been indications of OZI "violation" in the production of the ϕ and other supposedly pure $\bar{s}s$ mesons. For example, old bubble chamber data indicated that

$$\frac{\sigma(\bar{p}p \to \phi\pi^+\pi^-)}{\sigma(\bar{p}p \to \phi\pi^+\pi^-)} = (19 \pm 5) \times 10^{-3} \tag{2.52}$$

which is much larger than what could be expected from an admixture of $\bar{u}u$, $\bar{d}d$ components in the ϕ wave function, which is estimated to be around $(1 \div 4) \times 10^{-3}$ on the basis of mass formulae. The bubble chamber result eq. (2.52) corresponds to

$$0.05 < \left| \frac{\sqrt{2}\,\mathcal{A}(\bar{p}p \to \bar{s}s + X)}{\mathcal{A}(\bar{p}p \to \bar{u}u + X) + \mathcal{A}(\bar{p}p \to \bar{d}d + X)} \right| < 0.22 \tag{2.53}$$

In addition to this observation, early data indicated possible OZI violations in $\bar{p}n \to \phi\pi^-$, $\bar{p}p \to f_2'(1520)\pi^+\pi^-$, $pp \to pp\phi\ldots$ and $\Omega^* \to \Omega\pi\pi$ decay.

Among the proposed interpretations was OZI "evasion" [102] due to an $\bar{s}s$ component in the proton wave function, which provides the possibility of a new class of connected quark line diagrams as seen in Fig. 2.7. Additional evidence for this hypothesis may come from the presence of a backward peak in the reaction $\bar{p}p \to K^-K^+$ which could be due to the connected quark line diagram shown in Fig. 2.8, which involves the intrinsic strange component of the proton wave function.

An alternative explanation for "excess" ϕ production that has been proposed is rescattering through intermediate K, K^* states, but it has also been argued that any such effect would be too small, and subject to systematic cancellations. Yet another interpretation was proposed in terms of an exotic 1^{--} resonance $C(1480)$ previously reported in the $\phi\pi^0$ mass spectrum in the reaction $\pi^-p \to Cn$. However, it seems difficult to reconcile this interpretation with the final-state channel dependence seen more recently, and LEAR data do not confirm the existence of such a resonance.

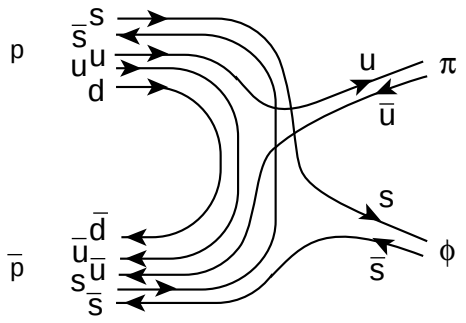

Figure 2.7: New class of connected quark line diagrams responsible for OZI "evasion" in $\bar{p}p \to \phi\pi$.

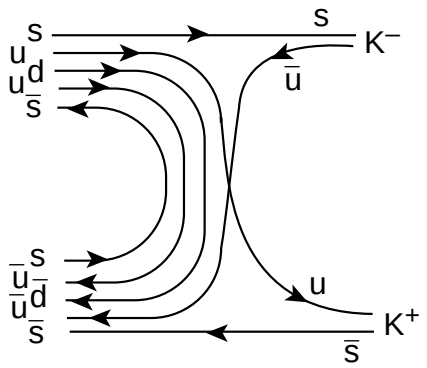

Figure 2.8: New class of connected quark line diagram which could account for the appearance of a backward peak in the reaction $\bar{p}p \to K^-K^+$.

It is also worth noticing that dispersion relation analyses of the proton vector isoscalar form factor also found suggestions of a surprisingly large $\phi\bar{p}p$ coupling [108–110] :

$$\frac{g^2_{\phi pp}}{g^2_{\omega pp}} \simeq 0.211 \text{ to } 0.276 \tag{2.54}$$

2.3 New Data from LEAR

The LEAR ring at CERN has provided large numbers of nucleon-antinucleon annihilations at or close to rest, which have enabled the OZI rule to be tested in ϕ production in association with many different final states X. The ASTERIX collaboration has measured the ratios of ϕX to ωX production for the states $X = \pi, \eta, \omega, \rho$ and $\pi\pi$, as reported in Table II.

TABLE II

The ratios $R = \phi X/\omega X$ for production of the ϕ and ω - mesons in antinucleon annihilation at rest. The parameter Z of the OZI-rule violation is calculated for $\delta = \Theta - \Theta_i = 3.7^0$, assuming identical phases of the ϕ and ω production amplitudes. The data are given for annihilation in liquid hydrogen target (percentage of annihilation from P-wave is $\sim 10-20\%$), gas target ($\sim$61% P-wave) and LX-trigger [111] ($\sim$86-91% P-wave).

Final state	Initial states	B.R.$\cdot 10^4$	$R \cdot 10^3$	$\lvert Z\rvert$ (%)	Comments
$\phi\gamma$	$^1S_0, ^3P_J$	0.17 ± 0.04	250 ± 89	42 ± 8	liquid, [112]
$\phi\pi^0$	$^3S_1, ^1P_1$	5.5 ± 0.7	96 ± 15	24 ± 2	liquid, [112]
$\phi\pi^0$		1.9 ± 0.5			gas, [111]
$\phi\pi^0$		0.3 ± 0.3			LX-trigger, [111]
$\phi\pi^-$	$^3S_1, ^1P_1$	9.0 ± 1.1	83 ± 25	22 ± 4	liquid, [113–116]
$\phi\pi^-$		14.8 ± 1.1	133 ± 26	29 ± 3	$\bar{p}d$, [117] †
$\phi\pi^-$			113 ± 30	27 ± 4	$\bar{p}d$, [117] ‡
$\phi\pi^+$			110 ± 15	26 ± 2	$\bar{n}p$, [117]
$\phi\eta$	$^3S_1, ^1P_1$	0.9 ± 0.3	6.0 ± 2.0	1.3 ± 1.2	liquid, [112]
$\phi\eta$		0.37 ± 0.09			gas, [111]
$\phi\eta$		0.41 ± 0.16			LX-trigger, [111]
$\phi\rho$	$^1S_0, ^3P_J$	3.4 ± 0.8	6.3 ± 1.6	1.4 ± 1.0	gas, [111,118]
$\phi\rho$		4.4 ± 1.2	7.5 ± 2.4	2.1 ± 1.2	LX-trigger, [111,118]
$\phi\omega$	$^1S_0, ^3P_{0,2}$	6.3 ± 2.3	19 ± 7	7 ± 4	liquid, [119,120]
$\phi\omega$		3.0 ± 1.1			gas, [111]
$\phi\omega$		4.2 ± 1.4			LX-trigger, [111]
$\phi\pi^0\pi^0$	$^{1,3}S_{0,1}, ^{1,3}P_J$	1.2 ± 0.6	6.0 ± 3.0	1.3 ± 2.0	liquid, [112]
$\phi\pi^-\pi^+$		4.6 ± 0.9	7.0 ± 1.4	1.9 ± 0.8	liquid, [121]
$\phi X, X = \pi^+\pi^-, \rho$		5.4 ± 1.0	7.9 ± 1.7	2.4 ± 1.0	gas, [111,118]
$\phi X, X = \pi^+\pi^-, \rho$		7.7 ± 1.7	11.0 ± 3.0	4.0 ± 1.4	LX-trigger, [111,118]

† $p < 200$ MeV/c
‡ $p > 400$ MeV/c

We see that there are large enhancements in S-wave annihilations as compared to naïve OZI rule, especially for the case $X = \pi$, whereas there are little or no enhancements in P-wave annihilations for $X = \pi, \eta, \rho, \pi\pi$. The Crystal Barrel collaboration has measured the corresponding ratios for $X = \pi^0, \eta, \pi^0\pi^0, \gamma$. As also seen in Table II, they confirm an enhancement over the OZI rule in

the case $X = \pi^0$, see no big effect in the cases $X = \eta, \pi^0\pi^0$, and find a very large enhancement in the case $X = \gamma$, which is about a hundred times the OZI prediction! The OBELIX collaboration also finds large enhancements in the cases $X = \pi^{\pm}$, as also seen in Table II.

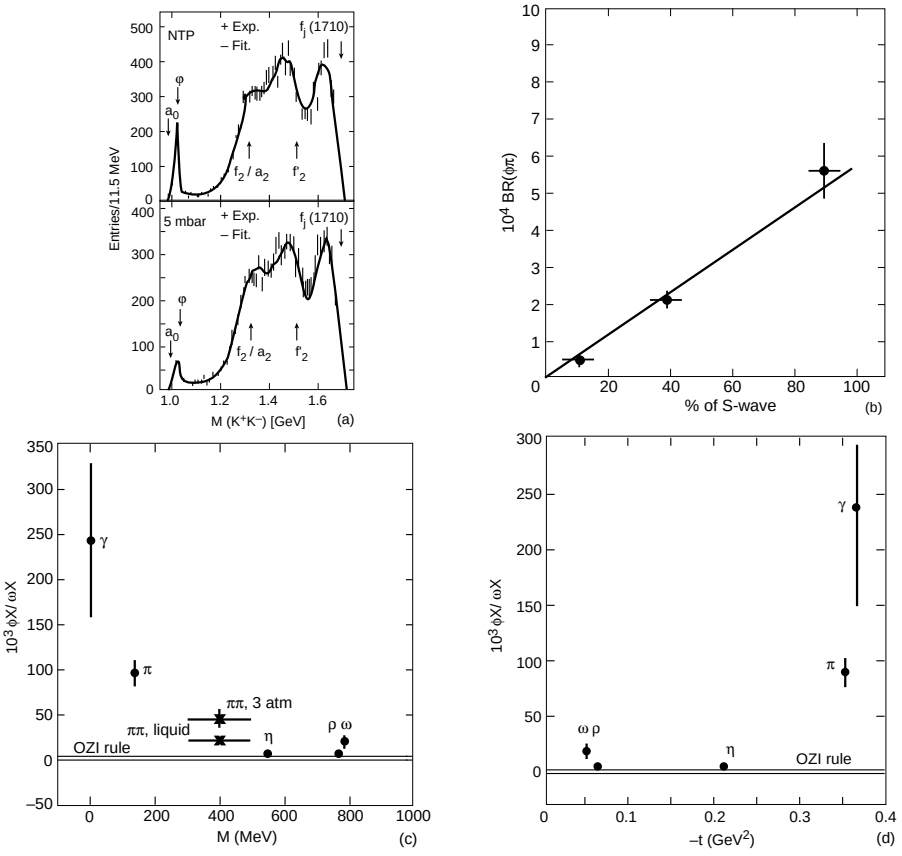

Figure 2.9: Recent experimental evidence from LEAR for breakdowns of the naïve OZI rule. (a) A ϕ peak is seen clearly in annihilations at NTP, but is less prominent at a pressure of 5 mbar, indicating (b) that $\phi\pi$ production is suppressed in P-wave annihilations. The amount of OZI "violation" depends on (c) the invariant mass of the system produced in association with the ϕ meson, and (d) the invariant momentum transfer to the ϕ.

Some interesting features of the available data are shown in Fig. 2.9. We see in Fig. 2.9a that $\phi\pi$ production is much smaller in P-wave annihilations than in

S-wave annihilations, and Fig. 2.9b shows that the $\pi\pi$ spectrum also depends on the partial wave. Fig. 2.9c shows the dependence of $\phi X/\omega X$ production ratios on the invariant mass of the system X, where we see progressively larger enhancements at smaller masses. Fig. 2.9d shows the corresponding ratios plotted versus the invariant momentum transfer t, where we see a large effect at large t.

These very interesting data exhibit the following features which need to be explained or accommodated in any model of OZI violation:

– Non-universal enhancement factors, which are strong for $X = \pi, \gamma$, smaller for $X = \rho, \omega, \pi\pi$, and not apparent for $X = \eta$.

– Larger enhancements in proton-antiproton annihilation at or near rest than in higher-energy annihilations, or in $\pi\pi$ and pp scattering.

– When the initial $\bar{p}p$ state is known, large enhancements are seen in S-wave annihilations into $X = \pi, \pi\pi$, but not in P-wave annihilations.

The next section introduces a model [82] which accommodates and explains these key features, and also makes some predictions for possible future experiments.

2.4 Model for a Polarized Strange Component in the Proton Wave Function

We consider [82] the likelihood that the Fock-space decomposition of the proton wave function contains an $\bar{s}s$ component which we parametrize as follows:

$$|p>= x \sum_X |uudX\rangle + z \sum_X |uud\bar{s}sX\rangle \tag{2.55}$$

where X denotes any combination of gluons and light $\bar{q}q$ pairs. As seen in Fig. 2.10, two important new classes of connected quark line diagrams become possible, the shake-out diagrams illustrated in Fig. 2.10a and the rearrangement diagrams illustrated in Fig. 2.10b. A typical shake-out amplitude may be estimated as

$$\mathcal{A}(\bar{p}p \to \bar{s}s + X) \simeq 2Re(xz^*)\ P(\bar{s}s), \tag{2.56}$$

where $P(\bar{s}s)$ is a projection factor which may depend on the final state, and perhaps also the initial state. A typical rearrangement amplitude may be estimated as

$$\mathcal{A}(\bar{p}p \to \bar{s}s + X) \simeq |z|^2\ T(\bar{s}s) \tag{2.57}$$

where $T(\bar{s}s)$ is another projection factor which is very likely to depend on the initial state: for example, naïve quark models might suggest that ϕ production would be enhanced in rearrangement of an initial S-wave $\bar{p}p$ state.

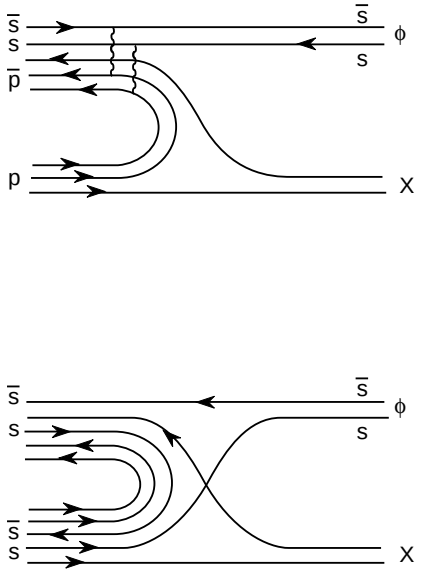

Figure 2.10: "Shakeout" and "rearrangement" diagrams responsible for ($\bar{p}p \to \bar{s}s + X$) in presence of an $\bar{s}s$ component in the proton wave function.

If we define the generic amplitude ratio

$$Z = \frac{\sqrt{2}\,\mathcal{A}(A + B \to \bar{s}s + X)}{\mathcal{A}(A + B \to \bar{u}u + X) + \mathcal{A}(A + B \to \bar{d}d + X)} \tag{2.58}$$

the measured production ratios are given by

$$R_X \equiv \frac{\sigma(\phi X)}{\sigma(\omega X)} \approx \left(\frac{Z + \tan\delta}{1 - Z\tan\delta}\right)^2 \times (\text{phase-space ratio}) \tag{2.59}$$

where δ is the angle representing the departure from ideal mixing in the vector meson nonet, which is a measure of the "expected" deviation from the OZI rule. We see from equation (2.55) that one might expect generic shake-out diagrams to yield

$$|Z| = 2\left|\frac{z}{x}\right| = 2\frac{|z|}{\sqrt{1 - |z|^2}} \tag{2.60}$$

assuming similar projection factors P, and generic rearrangement diagrams to

yield

$$|Z| = \left|\frac{z}{x}\right|^2 = \frac{|z|^2}{1-|z|^2} \tag{2.61}$$

assuming similar projection factors T. Data on S-wave π production correspond to

$$|Z(\phi\pi/\omega\pi)| = 0.24 \pm 0.02 \tag{2.62}$$

leading to the prediction

$$0.01 \leq |z|^2 \leq 0.19 \tag{2.63}$$

to the extent that the reactions are dominated by the shake-out and rearrangement mechanisms, respectively. These estimates are both compatible with data on K production in $\bar{p}p$ annihilation, which can be expected to contain a contribution from the higher Fock-space states in (2.55) as well as $\bar{s}s$ production in the final state:

$$Y_K = (4.74 \pm 0.22)\% \simeq 4[Re(xz^*)]^2 \tag{2.64}$$

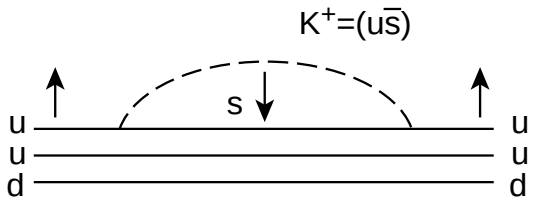

Figure 2.11: Emission of a K^+ meson in a chiral model, which may explain the negative polarization of s quarks in the proton wave function.

As we have seen in Lecture I, polarized structure function data indicate that the strange component of the proton wave function is polarized negatively: $\Delta s < 0$, and this feature should be incorporated in (2.55). Negative polarization of s quarks is understandable in a chiral model, as seen in Fig. 2.11. The emission of a K^+ flips the positive helicity of a u quark into negative polarization for an s quark. This argument does not provide immediately an indication on the possible polarization of an $\bar{s}s$ antiquark, but the simplest allowed possibility is

$$|uud\rangle_{\frac{1}{2},\frac{1}{2}} \ \oplus_{1,1} \ |\bar{s}s\rangle_{1,-1} \tag{2.65}$$

where there is a relative orbital angular momentum $|1,1\rangle$ between the two indicated components. The internal state of the $\bar{s}s$ pair is motivated by the fact that condensation in the vacuum occurs in a $^3P_0$ state.

Within this picture, one could expect that the rearrangement diagrams from a spin-triplet initial $\bar{p}p$ state would yield preferentially spin-triplet $\bar{s}s$ states such as the ϕ. One could also expect that S-wave $\bar{p}p$ annihilations would yield preferentially final states containing S-wave $\bar{s}s$ pairs. These arguments favour maximum ϕ production in $^3S_1$ annihilations, and less enhancement in $^1S_0$ and P-wave annihilations. A corollary would be the dilution of the ϕ enhancement at higher energies, where more partial waves contribute. Predictions for final states containing η mesons are more complicated, because more diagrams contribute since the η wave function contains both $\bar{q}q$ and $\bar{s}s$ components.

2.5 Future Tests of the Model

The following are some possible tests of these ideas for OZI evasion that could be tested in future experiments.

1. Production of the P-wave quark-model state $f'(1525)$ could be enhanced in P-wave $p\bar{p}$ annihilations, at least to the extent that they receive contributions from rearrangement diagrams. This suggestion already seems to be compatible with preliminary LEAR data.

2. A reduction in the enhancement of $\phi\pi/\omega\pi$ as the $\bar{p}$ momentum is increased, associated with the decreasing fraction of S-wave annihilations – for example, the S-wave fraction at $P_{\bar{p}} = 600$ MeV is between 14 and 20 %. This suggestion also seems to be compatible with data from the Crystal Barrel collaboration.

3. There should be considerable spin-dependence in the cross section for $p\bar{p} \to \phi\phi$, which should, for example, be higher from spin-triplet initial states.

4. Both S- and P-waves may contribute to the $\phi\pi\pi$ final state, and we would expect dominance by the $^3S_1$ initial state, which seems once more to be supported by recent data.

5. We would expect strong spin correlations in $p\bar{p} \to K^*\bar{K}^*$, which should be dominated by the $L = 0, S = 2$ state.

6. The large enhancement of $\phi\gamma/\omega\gamma$ observed should be dominated by the $^3P_{0,1,2}$ initial states, rather than the $^1S_0$ state.

7. The angular distribution of the e^+e^- pairs produced by ϕ decay in reactions of the type $p\bar{p} \to \phi + X$ should be

$$\sim (1 + \cos^2 \theta) \tag{2.66}$$

8. There should be significant dependence on the beam and target polarizations in the reaction $p+p \to p+p+\phi$, specifically, the cross section should be maximal when their polarizations are parallel. This effect should also be seen in the reaction $p+d \to {}^3\mathrm{He}+\phi$, where there are recent indications of a substantial enhancement of ϕ production relative to ω production and the naïve OZI rule.

9. The constituent counting rules

$$\left.\frac{d\sigma(A+B \to C+D)}{dt}\right|_{\substack{\theta_{CM} \\ \text{fixed}}} \simeq \frac{f(\theta_{CM})}{s^{n_A+n_B+n_C+n_D-2}} \tag{2.67}$$

suggest different behaviours for the reactions $\pi + p \to \phi, \omega + n$ at large momentum transfers. Specifically, the cross section for $\pi + p \to \phi + n$ should behave as s^{-12} if it is dominated by production from the $|uud\bar{s}s\rangle$ Fock state, or as s^{-9} if it is dominated by gluonic production. In either case, the ϕ/ω ratio should decrease at higher energies.

10. The different production mechanisms for $\phi\pi$ and $\omega\pi$, and for $\phi\,\pi\pi$ and $\omega\,\pi\pi$ final states, could lead to different angular distributions, as may be seen experimentally.

11. There should be a large enhancement in the Pontecorvo reaction $\bar{p} + d \to \phi + n$.

2.6 Extension of the Model to Λ Production

We finish this lecture by mentioning a couple of tests of these ideas [122,123] using data on Λ production in $p\bar{p}$ annihilation and elsewhere.

The total cross section for $p\bar{p} \to \Lambda\bar{\Lambda}$ and its angular distribution have been measured at LEAR by the PS 185 collaboration [124]. These have been described in terms of phenomenological models based on quarks and gluons, and on meson exchanges. The PS 185 data [124] indicate that the $\Lambda\bar{\Lambda}$ pairs are produced mainly in a spin-triplet state, as would be expected in our model (2.65), or in a gluon-exchange model [126], which produces a spin-triplet $s\bar{s}$ pair. Spin-triplet dominance can also be accommodated in a meson-exchange model [127], with the appropriate combination of K and K^* exchanges. Measurements

of the Λ depolarization D_{nn}, i.e., the transfer to the final-state Λ of polarization from a polarized p target, may help distinguish between different models [122].

Models which explain the EMC spin effect in terms of polarized gluons[21–23] would naturally expect that the gluon polarization is the same as the target p, and hence also that of the $s\bar{s}$ pair, and thus that of the Λ, so that $D_{nn} > 0$. On the other hand, the meson-exchange model has been used to predict $D_{nn} < 0$ [127]. On the other hand, in our polarized-strangeness model we would expect that the s in the proton wave function would have negative polarization, and hence that $D_{nn} < 0$ [122]. Thus the polarized-gluon and polarized-strangeness explanations of the EMC spin effect seem to predict opposite signs.

This idea can be extended to Λ production in the target fragmentation region of deep-inelastic lepton-nucleon scattering. Briefly stated, the proposal made in Ref. [123] is that a polarized lepton beam (a ν, $\bar{\nu}$, or a polarized μ or e) couples to the nucleon target preferentially through a particular boson (W or γ) polarization state, which then picks out preferentially a particular quark (or antiquark) polarization state. The target nucleon remnant "remembers" the spin that was removed, without the need for a polarized target. For example, if a positively-polarized u quark is removed from the proton wave function, it will tend to leave behind a negatively-polarized $s\bar{s}$ pair, which may lead to negative polarization for Λ's produced in the target fragmentation region [123], as also seen in Fig. 2.12.

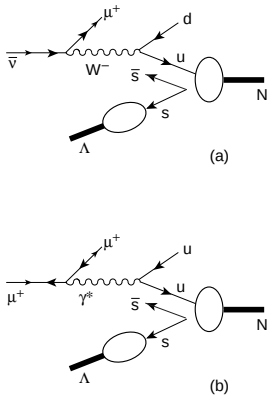

Figure 2.12: Diagrams which suggest that Λ baryons observed in the target fragmentation regions of deep-inelastic (a) $\bar{\nu}$ and (b) polarized μ^+ collisions should be polarized. The solid triangles represent the spin states of the various particles.

Just such an effect has been seen in the reaction $\bar{\nu} + N \rightarrow \mu^+ + \Lambda + X$

by the WA59 collaboration [125]. In the kinematic region $0.2 < x_{Bj} < 1$, $z < 0$, they measure

$$P_\Lambda = -0.85 \pm 0.19 \tag{2.68}$$

to be compared with the postdiction

$$P_\Lambda = -0.94D \tag{2.69}$$

in our model, where D is an uncalculable dilution factor. The comparison between equations (2.67) and (2.68) above indicates that $D = 0.9 \pm 0.2$. Similar predictions can be made, for example, for Λ's produced in the NOMAD ν experiment at CERN.

The fact that, according to the WA59 experiment, there does not seem to be dilution by a large factor encourages the extrapolation of these ideas to polarized $\mu(e)^+$ scattering, where we predict [123] that in the target fragmentation region

$$P_\Lambda = 0.7 P_{\mu(e)} D \tag{2.70}$$

This should be observable in the proposed HMC experiment at CERN, in the E665 experiment at Fermilab [128], and perhaps also in the HERMES [73] experiment at DESY.

3 Cosmological Spin-offs

In this lecture we discuss, as an example of the relevance of polarized structure function measurements and the spin decomposition of the nucleon to other areas of physics, their applications to experimental searches for dark matter particles. This discussion is prefaced by a brief review of the motivations for such particles.

3.1 How Much Dark Matter?

Naturalness and inflation [129] suggest that the density averaged over the universe as a whole should be very close to the critical density, which marks the boundary between a universe that expands forever and one which eventually collapses, i.e. $\Omega \equiv \rho/\rho_c \simeq 1$. On the other hand, the matter we can see shining in stars, in dust, etc. amounts only to $\Omega \simeq 0.01$ [130], as seen in Fig. 3.1. The agreement between big bang nucleosynthesis calculations [131] and the observed abundances of light elements suggests that $\Omega_{baryons} \lesssim 0.1$, as also seen in Fig. 3.1. This is to be compared with observations of rotation curves, which suggest according to the virial theorem that the amount of matter in galactic haloes $\Omega_{halo} \simeq 0.1$. A similar abundance of baryonic matters is suggested [130] by observations of rich clusters of galaxies.

Mathematically, the galactic haloes could in principle be purely baryonic, although they seem unlikely to be made out of gas, dust or "snow balls" [132]. However, there has recently been considerable interest in the possibility that haloes might be largely composed of "brown dwarfs". There have been several searches for such "failed stars" via microlensing of stars in the Large Magellanic Cloud [133] which indicate that

$$f = 0.20^{+0.33}_{-0.14} \tag{3.1}$$

be composed of brown dwarfs. This suggests that most of the dark matter present locally in our galactic halo

$$\rho_{halo} = 0.3 \text{ GeV/cm}^3 \times 1.5^{0\pm1} \tag{3.2}$$

is not baryonic in nature. Moreover, models of galaxy formation suggest that it is unlikely to be composed of massive neutrinos [134]. This leaves us only with the alternative of cold dark matter, whose detection involves in an essential way the spin decomposition of the nucleon, as we shall see later in this lecture.

Before addressing in more detail the nature of the dark matter, we first comment on the age and Hubble expansion rate of the Universe, which have recently generated some controversy. Globular clusters seem to be at least

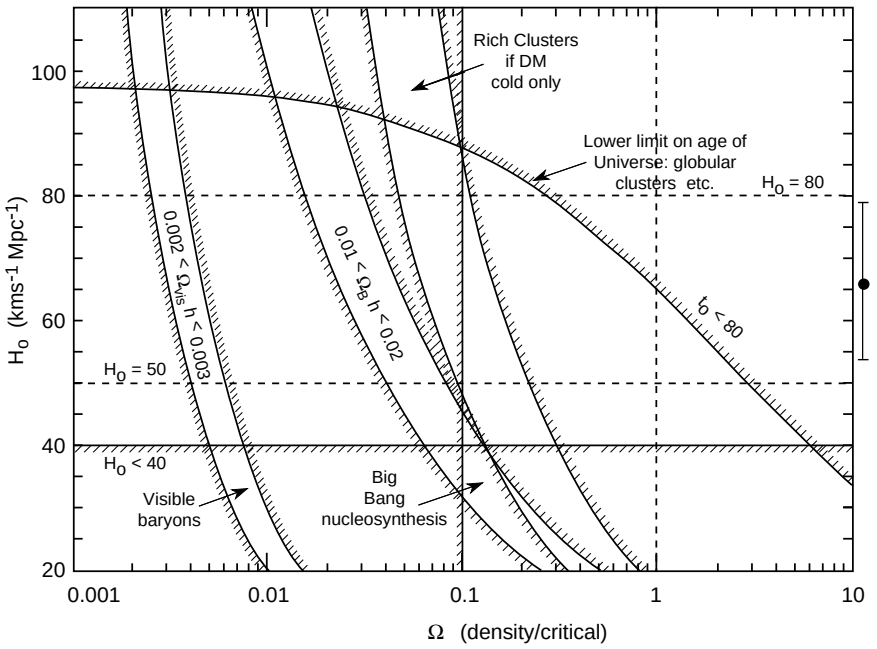

Figure 3.1: The (Ω, H_0) plane, adapted from[130], showing that there is no serious discrepancy between the average measured value of H_0, $\Omega = 1$, and an age for the Universe of 10^{10} years. This plot also shows the estimates of the present baryon density $\Omega_{baryons}$ obtained from visible features in the Universe, from Big Bang Nucleosynthesis [131] and from rich clusters. All the indications are that $\Omega_{baryons} \lesssim 0.1$, so that at least 90% of the matter in the Universe is non-baryonic dark matter.

14 ± 3 Gyr old, and nucleocosmochronology suggests an age of 13 ± 3 Gyr [130]. The question is whether these ages are compatible with current estimates of the Hubble constant H_0 km/sec/Mpc. Recent determinations of H_0 may be combined[135] to yield an estimate of 66 ± 13, which is shown on the vertical axis of Fig. 3.1. We see from this that there is no incompatibility between the age of the Universe being above 10^{10} yr old and $\Omega = 1$ as wanted by inflation [129]. However, if this is indeed the case, at least 90% of the matter in the universe must be unseen dark matter.

These terms refer to whether the dark matter was relativistic or non-relativistic at the cosmological epoch when structures such as galaxies and clusters began to form. Whether you favour hot or cold dark matter depends on your favourite theory of structure formation. If you believe that its origins lie in an approximately scale-invariant Gaussian random field of density perturbations, as suggested by inflationary models [136], then you should favour cold dark matter. This is because it enables perturbations to grow on all distance scales, whereas relativistic hot dark matter escapes from small-scale perturbations, whose growth via gravitational instabilities is thereby stunted [137]. Thus galaxies form later in a scenario based on Gaussian fluctuations and hot dark matter then they would in a scenario with cold dark matter. For this reason, the latter has commonly been regarded as the "standard model" of structure formation. However, if you believe that structures originated from seeds such as cosmic strings [138], then you should prefer hot dark matter, because cold dark matter would then give too much power in perturbations on small distance scales.

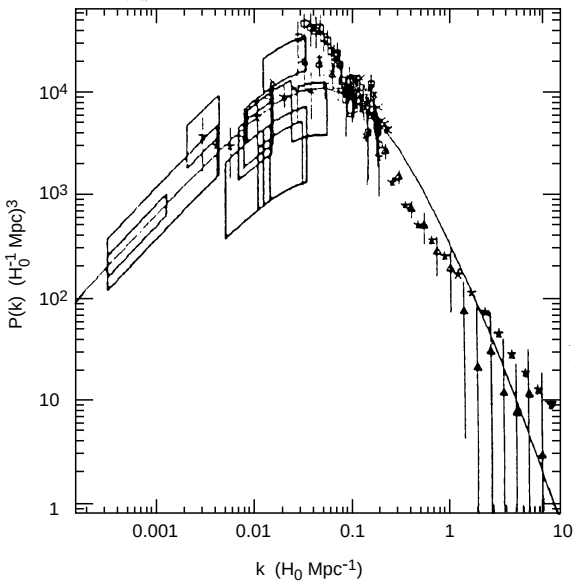

Figure 3.2: A compilation of data on the primordial perturbation spectrum [139], compared with a cold dark matter simulation assuming an initially scale-invariant spectrum of Gaussian fluctuations.

Fig. 3.2 shows a compilation [139] of data on the power spectrum of astrophysical perturbations, as obtained from COBE [140] and other observations of the cosmic microwave background radiation, and direct astronomical observations of galaxies and clusters. The solid line which does not quite pass through all the points is one calculated in the above-mentioned standard model of Gaussian fluctuations and cold dark matter. The discrepancies from this curve indicate that there is less perturbation power at small distances than would be expected in this theory, given the COBE normalisation at large distance scales.

This and other observations have suggested that it may be necessary to modify the pure cold dark matter model. Several suggestions have been offered, including a non-zero cosmological constant and a deviation of the spectrum of Gaussian perturbations from scale invariance. However, the preferred scenario seems to be an admixture of hot dark matter together with the cold, resulting in the following cocktail recipe for the Universe [141]:

$$\Omega_{cold} \simeq 0.7\,, \qquad \Omega_{hot} \simeq 0.2, \qquad \Omega_{baryons} \lesssim 0.1 \tag{3.3}$$

The way in which this scenario works is illustrated in Fig. 3.3. Hot dark matter

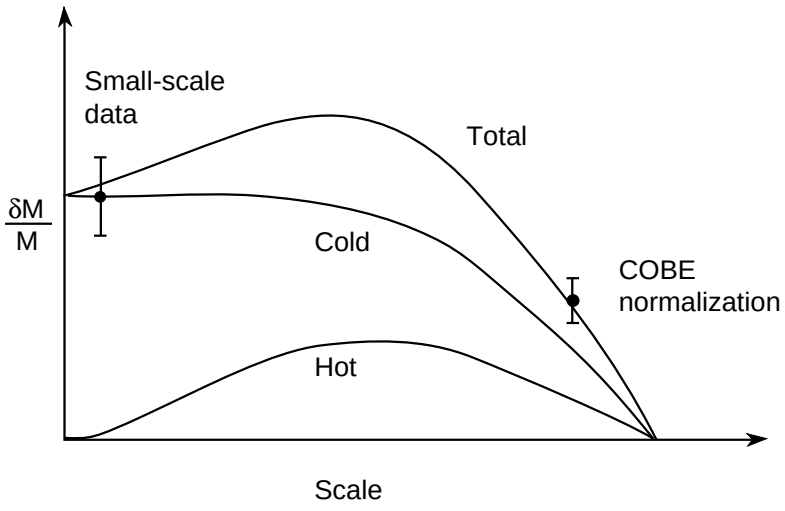

Figure 3.3: Illustration how a mixed dark matter scenario [141] may reconcile the large-scale perturbations seen by COBE [140] with the relatively small magnitude of the perturbations seen at small scales.

alone would give a spectrum of perturbations that dies out at small scales,

whereas hot dark matter does not. Combining the two, one can reconcile the relatively high COBE normalisation at large scales with the relatively small perturbations seen at small scales.

The only realistic candidate that particle physicists are able to offer for the hot dark matter is a neutrino weighing about 10 eV [142], but there are many candidates for the cold dark matter, of which we discuss two in the rest of this lecture.

3.3 Lightest Supersymmetric Particle

This is our favourite candidate for cold dark matter [143], and one for which the polarized structure function measurements are particularly relevant, as we shall see in the next section. The lightest supersymmetric particle (LSP) is expected to be stable in many models, and hence present in the Universe as a cosmological relic from the Big Bang. This is because supersymmetric particles possess a multiplicatively-conserved quantum number called R parity [144], which takes the values $+1$ for all conventional particles and -1 for all their supersymmetric partners. Its conservation is a consequence of baryon and lepton number cancelation, since

$$R = (-1)^{3B+L+2S} \tag{3.4}$$

There are three important consequences of R conservation:

1. Sparticles should always be produced in pairs.
2. Heavier sparticles should decay into lighter ones.
3. The LSP should be stable, since it has no legal decay mode.

If the LSP had electric charge or strong interactions, it would have condensed into galaxies, stars and planets such as ours, where it could in principle be detected in searches for anomalous heavy isotopes. Electromagnetic or strong interactions would bind such an LSP deeply inside some conventional nuclear species. Various searches have excluded such bound LSPs above the abundances [145]

$$\frac{n(\text{relics})}{n(\text{protons})} \sim 10^{-15} \text{ to } 10^{-30} \tag{3.5}$$

for 1 GeV $\lesssim m_{LSP} \lesssim$ 10 TeV, which are far below the abundances calculated for such relic particles, which usually lie in the range

$$\frac{n(\text{relics})}{n(\text{protons})} \gtrsim 10^{-6}\,(\text{em}) \quad \text{to} \quad 10^{-10}\,(\text{strong}) \tag{3.6}$$

We conclude [143] that any supersymmetric relic LSP should be electromagnetically neutral and possess only weak interactions. Scandidates in the future sparticle data book include the sneutrino $\tilde{\nu}$ of spin 0, some form of "neutralino" of spin 1/2, or the gravitino $\tilde{G}$ of spin 3/2. The sneutrino is essentially excluded by the LEP experiments which measured the decay of the Z^0 into invisible particles, which have counted the number of light neutrino species: 2.991 ± 0.0016 [146], which does not leave space for any sneutrino species weighing less than $\frac{1}{2}M_Z$, and by underground experiments to be discussed in the next section, which exclude a large range of heavier sneutrino masses. Since the gravitino is probably impossible to discover, and is anyway theoretically disfavoured as the LSP, we concentrate on the neutralino [143].

The neutralino χ is a mixture of the photino $\tilde{\gamma}$, the two neutral higgsinos $\tilde{H}^0_{1,2}$ expected in the minimal supersymmetric extension of the Standard Model, and the zino $\tilde{Z}$. This is characterized essentially by three parameters, the unmixed gaugino $m_{1/2}$, the Higgs mixing parameter μ, and the ratio of Higgs vacuum expectation values tan β. The phenomenology of the lightest neutralino is quite complicated in general, but simplifies in the limit $m_{1/2} \to 0$, where χ is approximately a photino state [147], and in the limit $\mu \to 0$, where it is approximately a higgsino state. As seen in Fig. 3.4, experimental constraints from LEP and the Fermilab collider in fact exclude these two extreme limits [148], so that

$$m_\chi \gtrsim (10 \text{ to } 20)\,\text{GeV} \tag{3.7}$$

Fig. 3.4 also indicates that there are generic domains of parameter space where the LSP may have an "interesting" cosmological relic density [149], namely

$$0.1 \lesssim \Omega_\chi H_0^2 \lesssim 1 \tag{3.8}$$

for some suitable choice of supersymmetric model parameters. Fig. 3.5 displays the calculated LSP density in a sampling of phenomenological models [150] where we see that an interesting cosmological density is quite plausible for LSP masses

$$20 \text{ GeV} \lesssim m_\chi \lesssim 300 \text{ GeV} \tag{3.9}$$

The next problem is how to detect the LSP, and this is where polarized structure function measurements may have a role to play.

3.4 Searches for Neutralinos

Several strategies to search for cosmological relic neutralinos have been proposed. One is to look for the products of their annihilations in our galactic halo [151]. Here the idea is that two self-conjugate χ particles may find each other

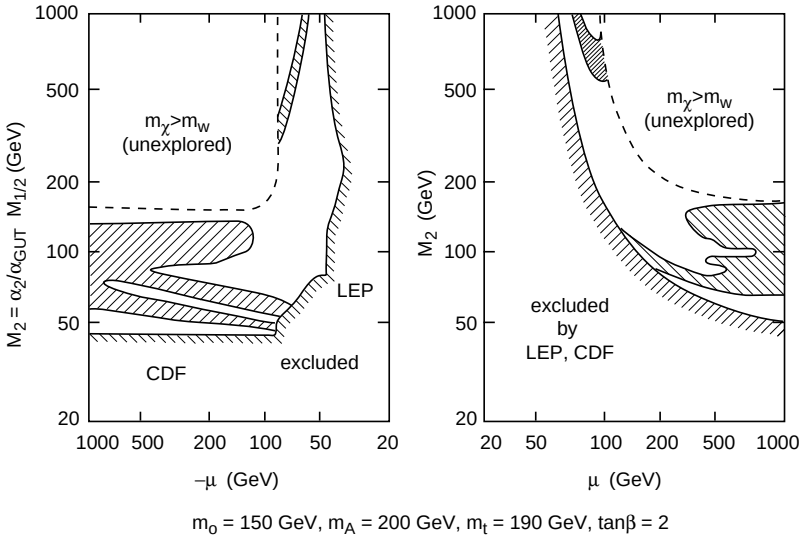

Figure 3.4: The cosmological relic density of neutralinos χ [143] may well (shaded regions) lie in the range of interest to astrophysicists and cosmologists [149], namely $0.1 \lesssim \Omega_\chi \lesssim 1$.

while circulating in the halo, and have a one-night stand and annihilate each other: $\chi\chi \to \ell\ell, \bar{q}q$, leading to a flux of stable particles such as $\bar{p}, e^+, \gamma, \nu$ in the cosmic rays. Several experiments have searched for cosmic-ray antiprotons [152], with the results shown in Fig. 3.5. At low energies there are only upper limits, but there are several positive detections at higher energies, which are comparable with the flux expected from secondary production by primary matter cosmic rays [153]. As also seen in Fig. 3.5, relic LSP annihilation in our galactic halo might produce an observable flux of low-energy cosmic ray antiprotons somewhat below the present experimental upper limits [154]. These may be interpreted as suggesting that

$$\rho_\chi \lesssim 10\, \rho_{halo} \tag{3.10}$$

NASA and the DOE have recently approved a satellite experiment called AMS [155], which should be able to improve significantly the present upper limits on low-energy antiprotons, and may be able to start constraining significantly supersymmetric models. It is also possible to derive limits on such models from the present experimental measurements of the cosmic-ray e^+ and γ fluxes [156], but these are not yet very constraining.

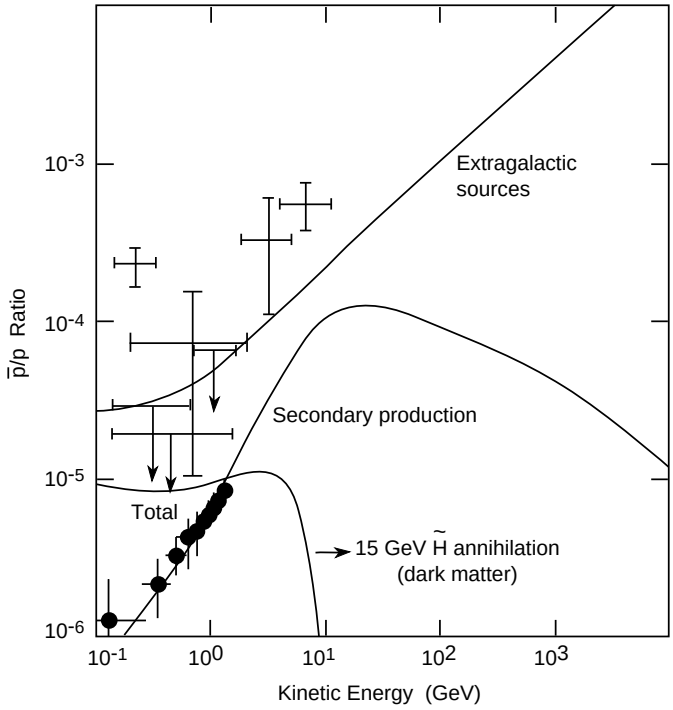

Figure 3.5: The results of experimental searches for cosmic-ray antiprotons [152], compared with the fluxes expected from primary matter cosmic rays [153] and a supersymmetric model[154]. The lower points with error bars are what should be obtainable with the AMS experiment[155].

A second LSP detection strategy is to look for $\chi\chi$ annihilation inside the Sun or Earth. Here the idea is that a relic LSP wandering through the halo may pass through the Sun or Earth [157], collide with some nucleus inside it, and thereby lose recoil energy. This could convert it from a hyperbolic orbit into an elliptic one, with a perihelion or perigee below the solar or terrestrial radius. If so, the initial capture would be followed by repeated scattering and energy loss, resulting in a quasi-isothermal distribution within the Sun or Earth. The resulting LSP population would grow indefinitely, à la Malthus, unless it were controlled either by emigration, namely evacuation from the surface, or by civil war, namely annihilation within the Sun or Earth. Evaporation is negligible for χ particles weighing more than a few GeV [158], so the only hope is annihilation.

The neutrinos produced by any such annihilation events would escape from the core, leading to a high-energy solar neutrino flux ($E_\nu \gtrsim 1$ GeV). This could be detected either directly in an underground experiment, or indirectly via a flux of upward-going muons produced by neutrino collisions in the rock.

The polarized structure function measurements enter in the estimate of the χ capture rate, which enters in the following general formula [159] for the neutrino flux:

$$R_\nu{=}2.7{\times}10^{-2} f\,(m_\chi/m_p)\left(\frac{\sigma(\chi p \to \chi p)}{10^{-40}\,\mathrm{cm}^2}\right)\left(\frac{\rho_\chi}{0.3\,\mathrm{GeV\,cm}^{-3}}\right)\left(\frac{300\ \mathrm{km\,s}^{-1}}{\bar{v}_\chi}\right){\times}F_\nu \tag{3.11}$$

where we have simplified to the case of capture by the Sun, where proton targets predominate. Here f is a kinematic function, ρ_χ and $\bar{v}_\chi$ are the local density and mean velocity of the halo LSPs, and F_ν represents factors associated with the neutrino interaction rate in the apparatus. The factor which interests us here is the elastic LSP-proton scattering cross section $\sigma(\chi\, p \to \chi\, p)$.

To see how the polarized structure functions enter into the estimation of the elastic scattering cross section [159], first note that the LSP interacts with hadrons via an effective four-fermion interaction of the general form $\chi\chi\bar{q}q$, which is mediated by the exchanges of massive particles such as the Z^0, Higgs bosons and squarks $\tilde{q}$, as seen in Fig. 3.6. This four-fermion interaction is simi-

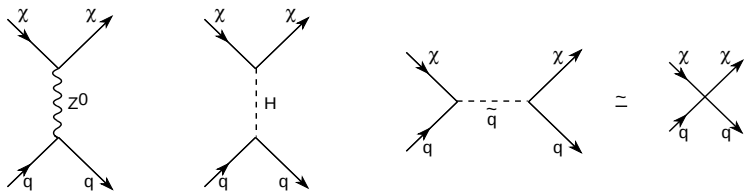

Figure 3.6: The exchanges of massive particle such as the Z^0, Higgs boson and squarks give rise to an effective four-fermion interaction between the neutralinos χ and quarks inside a proton target.

lar in many ways to the original Fermi four-fermion weak interaction mediated by $W^\pm$ exchange. The matrix elements of the latter interaction between nucleon states are governed by the familiar β-decay constant g_A, which may be written in the form

$$|g_A| = \Delta u - \Delta d \tag{3.12}$$

Analogous expressions in terms of the Δq exist for the spin-dependent part of the χ-nucleon scattering matrix element. For example, if the χ were to be a

pure photino state, we would have

$$a_p = \frac{4}{9}\Delta u + \frac{1}{9}\Delta d + \frac{1}{9}\Delta s \tag{3.13}$$

It is amusing to note that this is exactly the same combination of the Δq that appears in charged-lepton scattering off a proton target [159]. In a sense, the EMC and its successors have been measuring $\tilde{\gamma}$-nucleon scattering!

The EMC and subsequent measurements indicate values of the Δq that are rather different from those predicted by the naïve quark model, which means that the dark matter scattering matrix elements are also rather different, and hence also the upper limits on the halo dark matter density that can be deduced from a given search for high-energy neutrinos from the core of the Sun or the Earth. By now, as discussed in the first lecture, the determination of the Δq is quite precise, and, as discussed earlier in this lecture, we no longer believe that the LSP χ can be a pure $\tilde{\gamma}$. Consider, for example, the plausible case of an essentially pure $U(1)$ gaugino LSP $\tilde{B}$: its scattering matrix elements on protons and neutrons are given by [66]

$$\begin{aligned} a_p &\simeq \frac{17}{36}\Delta u + \frac{5}{36}(\Delta d + \Delta s) \\ a_n &\simeq (\Delta u \leftrightarrow \Delta d) \end{aligned} \tag{3.14}$$

We see that, in this case, the uncertainties [66] from polarized structure measurements are likely to be much smaller than those from other components in equation (3.11).

Some typical rate estimates for upward-going muons originating from high-energy solar neutrinos in a sampling of supersymmetric models are shown in Fig. 3.7:: while some models are already excluded by unsuccessful searches, most are not [150]. We see in Fig. 3.8 that searches for solar signals usually constrain models more than searches for terrestrial signals, though this is not a model-independent fact [150]. In the long run, it seems that a search for upward-going neutrino-induced muons with a 1 km^2 detector could almost certainly detect LSP annihilation [160], if most of the cold dark matter is indeed composed of LSPs.

The third LSP search strategy is to look directly for LSP scattering off nuclei in the laboratory [161]. It is easy to see that the typical recoil energy

$$\Delta E < m_\chi v^2 \simeq 10 \left(\frac{m_\chi}{10\,\mathrm{GeV}} \right) \mathrm{keV} \tag{3.15}$$

deposited by elastic χ-nucleus scattering would probably lie in the range of 10 to 100 keV. The type of spin-dependent interaction, mediated by Z^0 or $\tilde{q}$

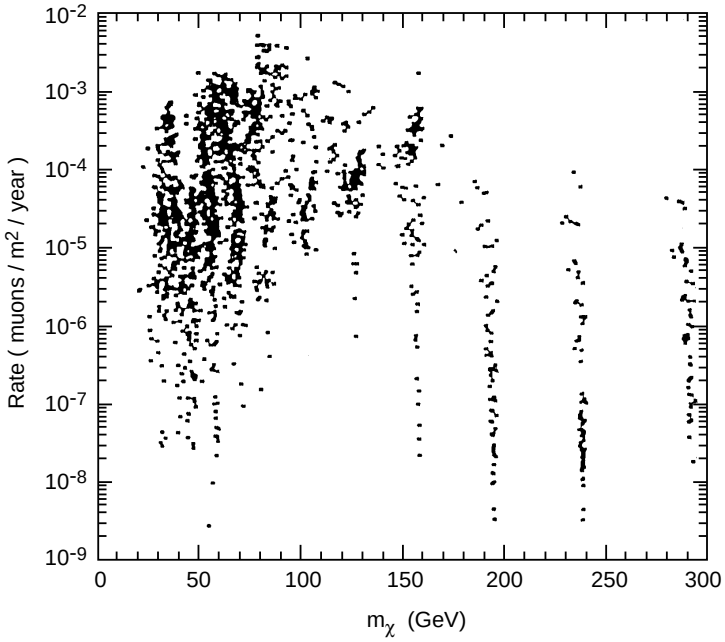

Figure 3.7: The flux of upward-going muons expected from $\chi\chi$ annihilation inside the Sun in a sampling of supersymmetric models [150].

exchange, that we discussed in previous paragraphs is likely to dominate for light nuclei [162], whereas coherent spin-dependent interactions mediated by H and $\tilde{q}$ exchange are likely to dominate scattering off heavy nuclei [163]. As we have already discussed, the spin-dependent interactions on individual nucleons are controlled by the Δq: translating these into matrix elements for interactions on nuclei depends on the decomposition of the nuclear spin, which must be studied using the shell model [162] or some other theory of nuclear structure [164]. The spin-independent interactions on individual nucleons are related to the different quark and gluon contributions to the nucleon mass, which is also an interesting phenomenological issue related to the π-nucleon σ-term discussed in Lecture II. Again, the issue of nuclear structure arises when one goes from the nucleon level to coherent scattering off a nuclear target.

We will not discuss here the details of such nuclear calculations, but present in Figs 3.9 and 3.10 the results of a sampling of different supersymmetric models [150]. We see in Fig. 3.9 that the spin-independent contribution tends to

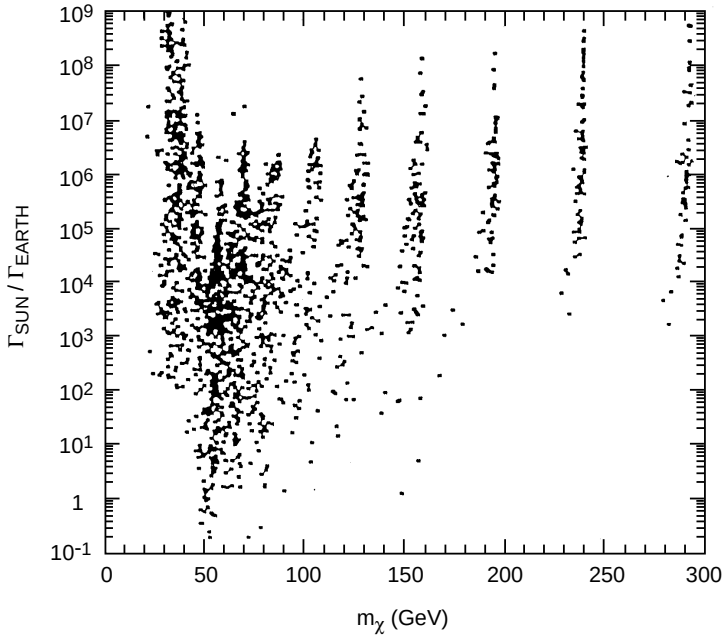

Figure 3.8: A comparison of the muon fluxes from the centre of the Sun and Earth, as found in a sampling of supersymmetric models [150].

dominate over the spin-dependent one in the case of Germanium, those this is not universally true, and would not be the case for scattering off Fluorine [162]. In Fig. 3.10 we plot the scattering rates off ^{73}Ge, where we see that there are many models in which more than 0.01 events/kg/day are expected, which may be observable. Thus the direct search for cold dark matter scattering in the laboratory may be a useful complement to the searches for supersymmetry at accelerators.

3.5 Axions

The axion [165] is our second-favourite candidate for the cold dark matter. It was invented to guarantee conservation of P and CP in the strong interactions, which would otherwise be violated by the θ parameter:

$$\mathcal{L}_{QCD} \ni \frac{\theta\, g^2}{32\pi^2}\, \epsilon^{\mu\nu\rho\sigma}\, G_{\mu\nu} G_{\rho\sigma} \tag{3.16}$$

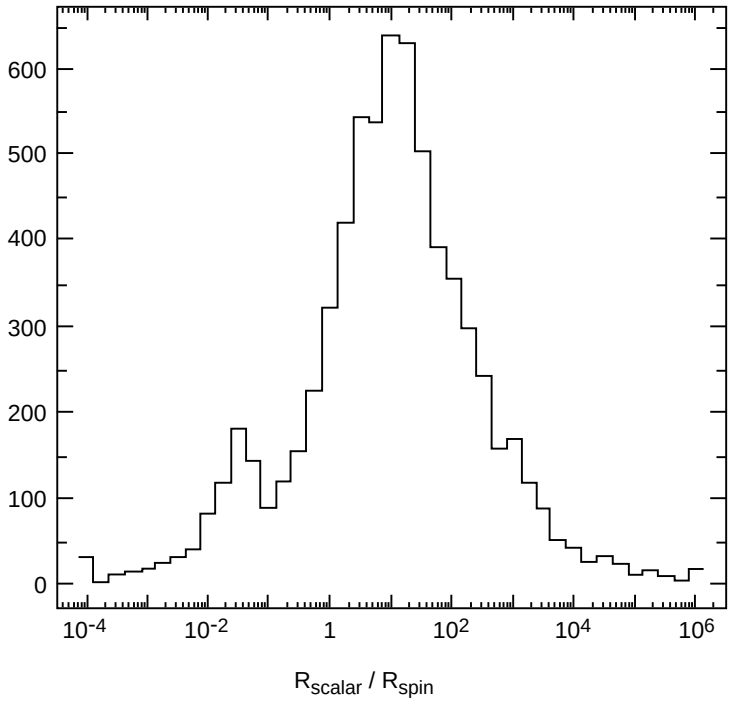

Figure 3.9: A comparison of the spin-dependent and spin-independent interaction rates of relic neutralinos χ with Germanium in a sampling of supersymmetric models [150].

which is known experimentally [2] to be smaller than about 10^{-9}. The θ parameter relaxes to zero in any extension of the Standard Model which contains the axion, a light pseudoscalar boson with mass and couplings to matter that are scaled inversely by the axion decay constant f_a:

$$m_a \sim \frac{\Lambda_{QCD}\, m_q}{f_a}\,, \quad g_{a\bar{f}f} \sim \frac{m_f}{f_a}\,, \qquad g_{a\gamma\gamma} \sim \frac{1}{f_a} \tag{3.17}$$

The fact that no axion has been seen in any accelerator experiment tells us that

$$f_a \gtrsim 1\,\mathrm{TeV} \tag{3.18}$$

and hence that any axion must be associated with physics beyond the scale of the Standard Model.

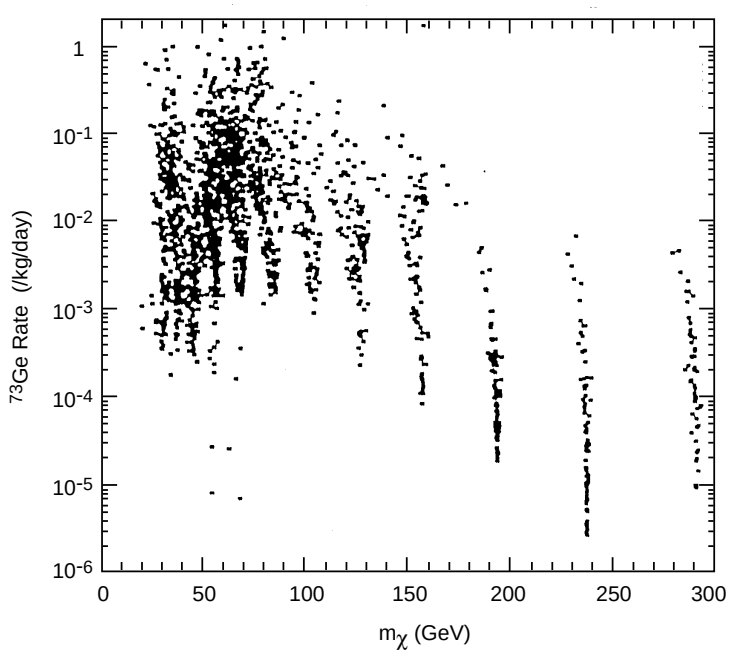

Figure 3.10: Total scattering rates on Germanium in a sampling of supersymmetric models [150].

Axions would have been produced in the early Universe in the form of slow-moving coherent waves that could constitute cold dark matter. The relic density of these waves has been estimated as [166]

$$\Omega_a \simeq \left(\frac{0.6 \times 10^{-5}\,\mathrm{eV}}{m_a}\right)^{7/6} \left(\frac{200\,\mathrm{MeV}}{\Lambda_{QCD}}\right)^{3/4} \left(\frac{75}{H_0}\right)^2 \tag{3.19}$$

which is less than unity if

$$f_a \lesssim 10^{12}\,\mathrm{GeV} \tag{3.20}$$

In addition to these coherent waves, there may also be axions radiated from cosmic strings [167], which would also be non-relativistic by now, and hence contribute to the relic axion density and strengthen the limit in equation (3.20).

The fact that the Sun shines photons rather than axions, or, more accurately but less picturesquely, that the standard solar model describes most

data, implies the lower limit [168]

$$f_a \gtrsim 10^7\,\mathrm{GeV} \tag{3.21}$$

This has been strengthened somewhat by unsuccessful searches for the axio-electric effect, in which an axion ionizes an atom. More stringent lower bounds on f_a are provided by the agreements between theories of Red Giant and White Dwarf stars with the observations [169] :

$$f_a \gtrsim 10^9\,\mathrm{GeV} \tag{3.22}$$

Between equations (3.20) and (3.22) there is an open window in which the axion could provide a relic density of interest to astrophysicists and cosmologists.

Part of this window may be closed by the observations of the supernova SN1987a, which is where the polarized structure function measurements come into play. According to the standard theory of supernova collapse to form a neutron star, 99% of the binding energy released in the collapse to the neutron star escapes as neutrinos. This theory agrees [170] with the observations of SN1987a made by the Kamiokande [171] and IMB experiments [172], which means that most of the energy could not have been carried off by other invisible particles such as axions.

Since the axion is a light pseudoscalar boson, its couplings to nuclear matter are related by a generalized Goldberger-Treiman relation to the corresponding axial-current matrix elements, and these are in turn determined by the corresponding Δq [173]. Specifically, we find for the axion couplings to individual nucleons that

$$\begin{aligned} C_{ap} &= 2[-2.76\,\Delta u - 1.13\,\Delta d + 0.89\,\Delta s - \cos 2\beta\,(\Delta u - \Delta d - \Delta s)]\,, \\ C_{an} &= 2[-2.76\,\Delta d - 1.13\,\Delta u + 0.89\,\Delta s - \cos 2\beta\,(\Delta d - \Delta u - \Delta s)] \end{aligned} \tag{3.23}$$

Evaluating the Δq at a momentum scale around 1 GeV, as is appropriate in the core of a neutron star, we estimate [66] that

$$\begin{aligned} C_{ap} &= (-3.9 \pm 0.4) - (2.68 \pm 0.06)\cos 2\beta \\ C_{an} &= (0.19 \pm 0.4) + (2.35 \pm 0.06)\cos 2\beta \end{aligned} \tag{3.24}$$

which are plotted in Fig. 3.11.

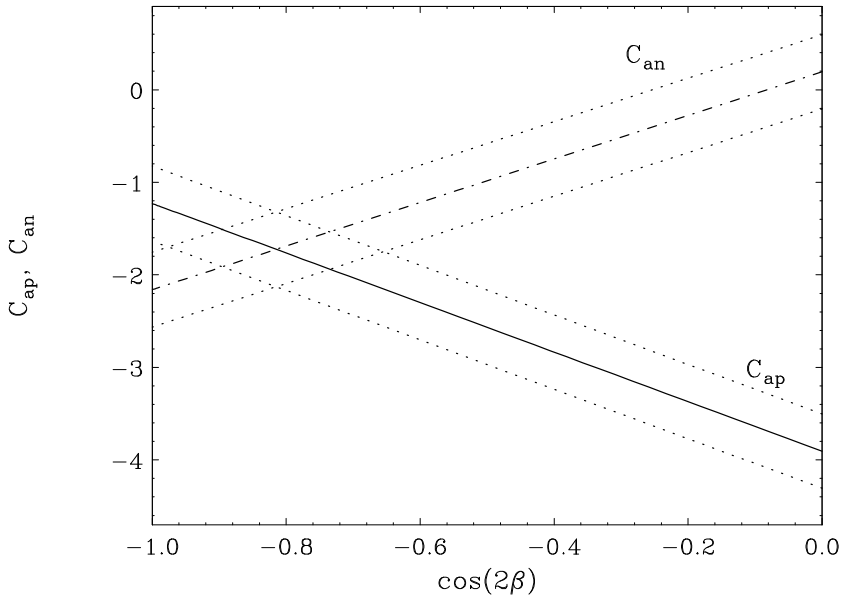

Figure 3.11: Axion couplings to the nucleon, as determined in Ref. [66] using polarized structure function data.

As in the case of LSP scattering, the uncertainties associated with polarized structure function measurements are by now considerably smaller than other uncertainties, in this case particularly those associated with the nuclear equation of state. The total axion emission rate from the core of a neutron star is approximately proportional to the combination

$$C_{an}{}^2 + 0.8\,(C_{an} + C_{ap})^2 + 0.5\,C_{ap}{}^2 \tag{3.25}$$

which is plotted in Fig. 3.12, together with the associated with the errors in the Δq. Estimating axion emission rates in this way [174], it seems that part of the previous axion window is still open, and an experiment [175] is underway which should be able to detect halo axions if they occupy this window.

3.6 The Role of Spin in the Forthcoming Revolutions in Particle Physics and Cosmology

Measurements of the spin decomposition may not only overturn our understanding of nucleon structure, but may also help usher in the revolutions in particle physics and cosmology for which we all yearn. A "Standard Model" for

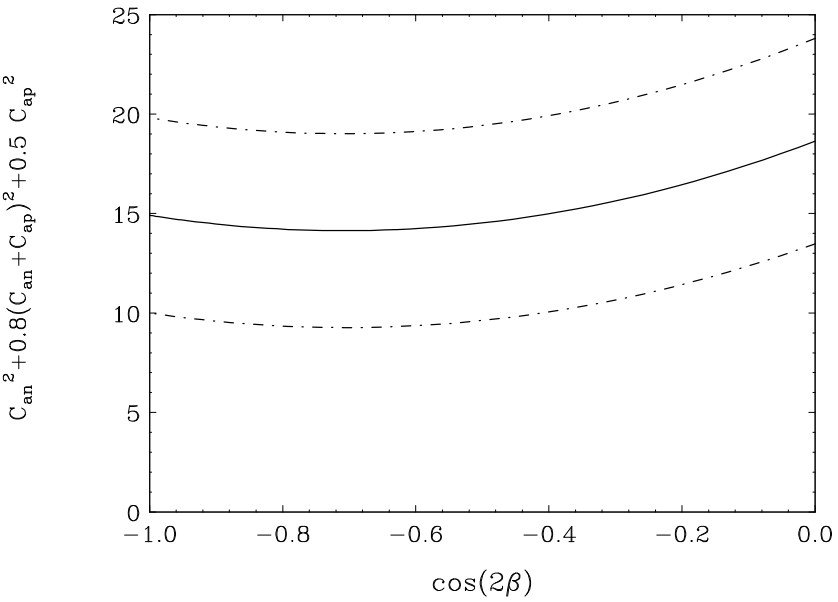

Figure 3.12: The total axion emission rate from the core of a neutron star, proportional to the combination $C_{an}{}^2 + 0.8\,(C_{an} + C_{ap})^2 + 0.5\,C_{ap}{}^2$, as determined in Ref. [66].

the formation of structure in the Universe is now emerging, in which Gaussian perturbations laid down during an inflationary epoch are amplified by gravitational instabilities fed by cold dark matter particles. The COBE observations of primordial fluctuations in the microwave background spectrum [140] were perhaps the first observational evidence for this picture, just as the discovery of neutral currents heralded the establishment of the Standard Model of elementary particles. Confirmation of this emerging picture of structure formation would be provided by the observation of one or more species of dark matter particle, such as massive neutrinos and LSPs or axions. The discovery of any of these would also cause a revolution in particle physics by taking us finally beyond the Standard Model, as well as telling us how galaxies and clusters were formed. As we have seen in this last lecture, polarized structure function measurements control the couplings to matter of both LSPs and axions, and could well play an important role in their detection.

Long live the Spin Revolution!

Acknowledgements

We thank Michelle Mazerand for her help in preparing the manuscript. The research described in these lectures was supported in part by the Israel Science Foundation administered by the Israel Academy of Sciences and Humanities, and by a Grant from the G.I.F., the German-Israeli Foundation for Scientific Research and Development.

1. J. Ellis and M. Karliner, *Nucleon Spin*, hep-ph/9510402, invited plenary talk at the Workshop on Deep Inelastic Scattering and QCD, Paris, April 1995
2. Particle Data Group, Review of Particle Properties, *Phys. Rev.* **D50**(1994)1173.
3. S.Y. Hsueh *et al.*, *Phys. Rev.* **D38**(1988)2056.
4. J. Lichtenstadt and H.J. Lipkin, *Phys. Lett.* **B353**(1995)119.
5. J. Ellis and M. Karliner, *Phys. Lett.* **B213**(1988)73.
6. D. B. Kaplan and A. Manohar, *Nucl. Phys.* **B310**(1988)527.
7. L.A. Ahrens *et al.*, *Phys. Rev.* **D35**(1987)785.
8. G. Garvey, private communication.
9. W.M. Alberico *et al.*, *Elastic νN and $\bar{\nu} N$ scattering and strange form-factors of the nucleons*, hep-ph/9508277.
10. J. Bjorken, *Phys. Rev.* **148**(1966)1467; **D1**(1970)1376.
11. J. Ellis and R.L. Jaffe,*Phys. Rev.* **D9**(1974)1444; **D10**(1974)1669.
12. J. Kodaira *et al.*, *Phys. Rev.* **D20**(1979)627; J. Kodaira *et al.*, *Nucl. Phys.* **B159**(1979)99.
13. S.A. Larin, F.V. Tkachev and J.A.M. Vermaseren, *Phys. Rev. Lett.* **66**(1991)862; S.A. Larin and J.A.M. Vermaseren, *Phys. Lett.* **B259**(1991)345.
14. S.A. Larin, *Phys. Lett.* **B334**(1994)192.
15. SLAC-Yale E80 Collaboration, M.J. Alguard *et al.*, *Phys. Rev. Lett.* **37**(1976)1261; **41**(1978)70.
16. SLAC-Yale Collaboration, G. Baum *et al.*, *Phys. Rev. Lett.* **45**(1980)2000;
17. SLAC-Yale E130 Collaboration, G. Baum *et al.*, *Phys. Rev. Lett.* **51**(1983)1135;
18. The EMC Collaboration, J. Ashman *et al.*, *Phys. Lett.* **B206**(1988)364; *Nucl. Phys.* **B328**(1989)1.
19. R.L. Heimann, *Nucl. Phys.* **B64**(1973)429.
20. S.J. Brodsky, J. Ellis and M. Karliner, *Phys. Lett.* **B206**(1988)309.
21. A.V. Efremov and O.V. Teryaev, Dubna report, JIN-E2-88-287(1988).
22. G Altarelli and G. Ross, *Phys. Lett.* **B212**(1988)391.

23. R. D. Carlitz, J.D. Collins and A.H. Mueller, *Phys. Lett.* **B214**(1988)229.
24. G.M. Shore and G. Veneziano, *Phys. Lett.* **B244**(1990)75.
25. G.M. Shore and G. Veneziano, *Nucl. Phys.* **B381**(1992)23.
26. S. Narison, G.M. Shore and G. Veneziano *Nucl. Phys.* **B433**(1995)209.
27. E143 Coll., K. Abe *et al.*, *Measurements of the Q^2 Dependence of the Proton and Deuteron Spin Structure Functions g_1^p and g_1^d*, SLAC-PUB-95-6997, hep-ex/9511015.
28. G. Altarelli, P. Nason and G. Ridolfi, *Phys. Lett.* **B320**(1994)152, erratum – *ibid.*, **B325**(1994)538.
29. R.D. Ball, S. Forte, G. Ridolfi, *Nucl. Phys.* **B444**(1995)287, E – *ibid* **B449**(1995)680.
30. B. Ehrnsperger and A. Schäfer, *Phys. Rev.* **D52**(1995).
31. D. de Florian *et al.*, *Scale dependence of polarized DIS asymmetries*, hep-ph/9505377.
32. T. Gehrmann and W.J. Stirling, *Analytic approaches to the evolution of polarized parton distributions at small x*, hep-ph/9507332.
33. M. Glück *et al.*, *Next-to-leading order analysis of polarized and unpolarized structure functions*, hep-ph/9508347.
34. R.D. Ball, S. Forte, G. Ridolfi, *Next-to-leading Order Determination of the Singlet Axial Charge and the Polarized Gluon Content of the Nucleon*, CERN-TH-95-266, hep-ph/9510449.
35. T. Gehrmann and W.J. Stirling, *Polarized Parton Distributions in the Nucleon*, Durham preprint DTP/95/82, hep-ph/9512406.
36. A. De Rujula, S.L. Glashow, H.D. Politzer, S.B. Treiman, F. Wilczek and A. Zee, *Phys. Rev.* **D10**(1974)1649.
37. S.J. Brodsky, J. Ellis and M. Karliner, unpublished.
38. R.D. Ball and S. Forte, *Nucl. Phys.* **B444**(1995)287, E – *ibid.* **B449**(1995)680.
39. J. Bartels, B.I. Ermolaev and M.G. Ryskin, *Nonsinglet contributions to the structure function g_1 at small x*, hep-ph/9507271.
40. S.D. Bass and P.V. Landshoff, *Phys. Lett.* **B336**(1994)537.
41. F.E. Close and R.G. Roberts, *Phys. Lett.* **B336**(1994)257.
42. M.G. Doncel and E. de Rafael, Nuovo Cimento **4A** (1971) 363.
43. SMC Coll., D. Adams *et al.*, *Phys. Lett.* **B336**(1994)125.
44. E143 Coll., K. Abe *et al.*, SLAC-PUB-95-6982(1995).
45. S. Wandzura and F. Wilczek, *Phys. Lett.* **B72**(1977)195.
46. H. Burkhardt and W.N. Cottingham, *Ann. Phys.* **56**(1970)453.
47. G. Altarelli *et al.*, *Phys. Lett.* **B334**(1994)187.
48. J. Kodaira *et al.*, *Phys. Lett.* **B345**(1995)527.
49. A. Mueller *Nucl. Phys.* **B250**(1985)327; A.I. Vainshtein and V.I. Za-

kharov, *Phys. Rev. Lett.* **73**(1994)1207.
50. C. Sachrajda, *Renormalons*, hep-lat/9509085.
51. G. Grunberg, *Phys. Lett.* **95B**(1980)70, E – *ibid.* **110B**(1982)501; *Phys. Rev.* **D29**(1984)2315; P.M. Stevenson, *Phys. Rev.* **D23**(1981)2916;
52. A. L. Kataev and V. V. Starshenko, *Mod.Phys.Lett.* **A10**(1995)235.
53. S.J. Brodsky, G.P. Lepage and P.M. Mackenzie, *Phys. Rev.* **D28**(1983)228.
54. S.J. Brodsky and H.J. Lu, *Phys. Rev.* **D51**(1995)3652.
55. M.A. Samuel, J. Ellis and M. Karliner, *Phys. Rev. Lett.* **74**(1995)4380.
56. J. Ellis, E. Gardi, M. Karliner and M.A. Samuel, *Padé Approximants, Borel Transforms and Renormalons: the Bjorken Sum Rule as a Case Study*, hep-ph/9509312, to be published in *Phys. Lett. B*.
57. G.A. Baker, Jr. *Essentials of Padé Approximants*, Academic Press, 1975.
58. C.M. Bender and S.A. Orszag, *Advanced Mathematical Methods for Scientists and Engineers*, McGraw-Hill, 1978.
59. M.A. Samuel, G. Li and E. Steinfelds, *Phys. Rev.* **E51**(1995)3911; M.A. Samuel and S.D. Druger, *Intl. J. Th. Phys.* **34**(1995)903.
60. C.N. Lovett-Turner and C.J.Maxwell *Nucl. Phys.* **B432**(1994)147.
61. C.N. Lovett-Turner and C.J. Maxwell, *Nucl. Phys.* **B452**(1995)188.
62. G. Grunberg, *Phys. Lett.* **B325** (1994) 441; see also V.A. Fateev, V.A. Kazakov and P.B. Wiegmann, *Nucl. Phys.* **B424**(1994)505 for a 2-dimensional example where this prescription is exact.
63. S.J. Brodsky, J. Ellis, E. Gardi, M. Karliner and M. Samuel, to be published.
64. J. Collins, *The Problem Of Scales: Renormalization and All That*, hep-ph/9510276, lectures at TASI 95.
65. I.I. Balitsky, V.M. Braun and A.V. Kolesnichenko, *Phys. Lett.* **B242**(1990)245; erratum: *ibid*, **B318**(1993)648. B. Ehrnsperger, A. Schäfer and L. Mankiewicz, *Phys. Lett.* **B323**(1994)439; G.G. Ross and R.G. Roberts, *Phys. Lett.* **B322**(1994)425; E. Stein *et al.*, *Phys. Lett.* **B343**(1995)369; E. Stein *et al.*, *Phys. Lett.* **B353**(1995)107.
66. J. Ellis and M. Karliner, *Phys. Lett.* **B341**(1995)397.
67. V.M. Braun, *QCD Renormalons and Higher Twist Effects*, Proc. Moriond 1995, hep-ph/9505317.
68. SMC Coll., B. Adeva *et al.*, *Phys. Lett.* **B302**(1993)533; E142 Coll., P.L. Anthony *et al.*, *Phys. Rev. Lett.* **71**(1993)959; SMC Coll., D. Adams *et al.*, *Phys. Lett.* **B329**(1994)399; E143 Coll., K. Abe *et al.*, *Phys. Rev. Lett.* **74**(1995)346, *Phys. Rev. Lett.* **75**(1995)25; SMC Coll., D. Adams *et al.*, *Phys. Lett.* **B357**(1995)248.
69. P. Grenier, Ph.D. dissertation (1995) and private communication.

70. Y. Roblin, Ph.D. dissertation (1995).
71. S. Bethke, Aachen preprint PITHA-95-14 (1995), in *Proc. 30-th Rencontre de Moriond, QCD and High-Energy Hadronic Interactions*.
72. M. Schmelling, *Measurements of α_s and Tests of the Structure of QCD*, CERN-PPE/95-129, in *Proc. Physics in Collision*, Cracow, Poland, June 8-10, 1995.
73. For a recent detailed description, see M. Duren, *The HERMES Experiment: From the Design to the First Results*, Ph.D. dissertation, DESY-HERMES-95-02, Jul 1995.
74. V. Hughes, these *Proceedings*.
75. D. B. Kaplan, Phys. Lett. B**235**, 163 (1990); Nucl. Phys. B**351**, 137 (1991).
76. H. Fritzsch, *Phys. Lett.* **B256**, 75 (1991) and Proc. Bad Honnef Workshop 1992, K. Goeke *et al.*, Eds., Springer-Verlag, 1993.
77. J. Ellis, Y. Frishman, A. Hanany, and M. Karliner, Nucl. Phys. **B382**(1992)189.
78. G. Gomelski, M. Karliner and S.B. Selipsky, *Phys. Lett.* **B323**(1994)182.
79. K. Steininger and W. Weise, *Phys. Rev.* **D48**(1993)1433.
80. Y. Frishman, Y. Hanany and M. Karliner, *Nucl. Phys.* **B424**(1994)3, and preprint *On the Stability of Quark Solitons in QCD*, hep-ph/9507206.
81. G. Altarelli, S. Petrarca and F. Rapuano, *The Pion Structure Function in a Constituent Model*, CERN-TH/95-273, hep-ph/9510346.
82. J. Ellis, M. Karliner, D.E. Kharzeev and M.G. Sapozhnikov, *Phys. Lett.* **B353**(1995)319.
83. J. Ellis, R. Flores and S. Ritz, *Phys. Lett.* **198B**(1987)393.
84. T-P. Cheng and L-F. Li, *Gauge Theory of Elementary Particle Physics*, Clarendon Press, 1984.
85. J. Gasser and H. Leutwyler *Phys. Rep.* **87**(1982)77.
86. G. 't Hooft *Nucl. Phys.* **B72**(1974)461; **B75**(1974)461.
87. T.H.R. Skyrme *Proc. Roy. Soc. London* **A260**(1961)127.
88. E. Witten, *Nucl. Phys.* **B160**(1979)57.
89. E. Witten, *Nucl. Phys.* **B223**(1983)422, *ibid*, 433.
90. G. Adkins, C. Nappi and E. Witten, *Nucl. Phys.* **B228**(1983)433.
91. For the 3 flavour extension of the model see: E. Guadagnini, *Nucl. Phys.* **236**(1984)35; P. O. Mazur, M. A. Nowak and M. Praszałowicz, *Phys. Lett.* **147B**(1984)137.
92. For a review of the Skyrme model and its phenomenology see I. Zahed and G.E. Brown, *Phys. Rept.* **142**(1986)1; B. Schwesinger *et al.*, *Phys. Rept.* **173**(1989)173.
93. E. Witten in Lewes Workshop Proc.; A. Chodos *et al.*, Eds; Singapore,

World Scientific, 1984.
94. G.D. Date, Y. Frishman and J. Sonnenschein, *Nucl. Phys.* **B283**(1987)365.
95. Y. Frishman and M. Karliner, *Nucl. Phys.* **B334**(1990)339.
96. S. L. Adler, *Phys. Rev.* **177**(1969)2426); J. S. Bell and R. Jackiw, *Nuov. Cim.* **A51**(1967)47.
97. E. Witten, *Nucl. Phys.* **B156**(1979)269; G. Veneziano, *Nucl. Phys.* **B159**(1979)213; P. di Vecchia and G. Veneziano, *Nucl. Phys.* **171**(1980)253; P. di Vecchia, F. Nicodemi, R. Pettorino and G. Veneziano, *Nucl. Phys.* **B181**(1981)318.
98. M. Karliner and M.P. Mattis, *Phys. Rev. Lett.* **56**(1986)428.
99. J. Donoghue and C. Nappi, *Phys. Lett.* **B168**(1986)105.
100. M. P. Mattis and M. Karliner, *Phys. Rev.* **D31**(1985)2833; *ibid* **D34**(1986)1991; *Phys. Rev. Lett.* **56**(1986)428; M. P. Mattis and M. Peskin, *Phys. Rev.* **D32**(1985)58; M. Karliner *Phys. Rev. Lett.* **57**(1986)523; M. Karliner and M.P. Mattis, *Phys. Rev.* **D34**(1986)1991.
101. A. Hayashi, G. Eckart, G. Holzwarth and H. Walliser, *Phys. Lett.* **147B**(1984)5; H. Walliser and G. Eckart, *Nucl. Phys.* **A429**(1984)514.
102. J. Ellis, E. Gabathuler and M. Karliner, Phys.Lett.**B217**(1989)173.
103. FNAL E581/704 Collaboration, D.L. Adams *et al.*, *Phys. Lett.* **B336**(1994)269.
104. R.L. Jaffe, *Gluon spin in the Nucleon*, MIT-CTP-2466, hep-ph/9509279.
105. S. Okubo, *Phys. Lett.* **5**(191963)165; G. Zweig, CERN Report No. 8419/TH412, (1964 (unpublished); I. Iuzuka, *Prog. Theor. Phys. Suppl.* **37-38**(1966)21; see also G. Alexander, H.J. Lipkin and P. Scheck, *Phys. Rev. Lett.* **17**(191966)412.
106. T.P. Cheng, *Phys. Rev.* **D13**(1976)2161.
107. J. Gasser, M.E. Sainio and A. Švarc, *Nucl. Phys.* **B307**(1988)779; M. E. Sainio, *Update of the σ term*, Helsinki report HU-TFT-95-36, Jul 1995, invited talk at 6-th International Symposium on Meson - Nucleon Physics and Structure of the Nucleon, Blaubeuren, Germany, 10-14 Jul 1995.
108. G. Höhler *et al.*, *Nucl.Phys.* **B114**(1976)505.
109. S. Dubnicka, *Nuov. Cim.* **A100**(1988)1.
110. R.L. Jaffe, *Phys. Lett.* **B229**(1989)275; H. Forkel, *Strangeness in the Nucleon: the Strange Form Factors*, ECT*/Dec/95-004, hep-ph/9512326.
111. The ASTERIX Collaboration, J. Reifenrother *et al.*, *Phys. Lett.* **B267**(1991)299.
112. The Crystal Barrel Collaboration, M.A. Faessler *et al.*, Proc. NAN-93 Conference, Moscow, 1993; *Phys. At. Nuclei* **57** (1994) 1693.
113. R. Bizzarri *et al.*, *Nuov. Cim.* **A20**(1974) 393.

114. A. Bettini *et al.*, *Nuov. Cim.* **A63**(1969) 1199.
115. R. Bizzarri *et al.*, *Phys. Rev. Lett.* **25**(1970) 1385.
116. A. Bettini *et al.*, *Nuov. Cim.* **A47**(1967) 642.
117. The OBELIX Collaboration, V.G. Ableev *et al.*, Proc. NAN-93 Conference, Moscow, 1993; *Phys. At. Nuclei* **57** (1994) 1716.
118. The ASTERIX Collaboration, P. Weidenauer *et al.*, *Z.Phys.* **C59**(1993)387.
119. R. Bizzarri *et al.*, *Nucl. Phys.* **B27** (1971)140.
120. The Crystal Barrel Collaboration, C. Amsler *et al.*, *Z.Phys.* **C58**(1993)175.
121. R. Bizzarri *et al.*, *Nucl. Phys.* **B14**(1969)169.
122. M. Alberg, J. Ellis, D. Kharzeev, *Phys. Lett.* **B356**(1995)113.
123. J. Ellis, D. Kharzeev and A. Kotzinian, *The proton spin puzzle and* Λ *polarization in deep inelastic scattering*, CERN-TH-95-135, hep-ph/9506280.
124. The PS185 Collaboration, P. Barnes *et al.*, *Nucl. Phys.* **A526** (1991) 575; *Phys. Lett.* **B229** (1989) 432; *Phys. Lett.* **B189** (1987) 249.
125. S. Willocq *et al.*(WA59 Collaboration), *Z. Phys.* **C53** (1992) 207.
126. H.R. Rubinstein and H. Snellman, *Phys. Lett.* **B165** (1985) 187.
127. F. Tabakin and R. Eisenstein, *Phys. Rev.* **C31** (1985) 1857.
128. D. Ashery, *"Measurement of* Λ *Polarizarion and the Spin Structure of the* Λ *and the Nucleon"*, private communication and proposal submitted to the BSF (1995).
129. A.A. Starobinsky, *Phys. Lett.* **91B** (1980) 99; A. Guth, *Phys. Rev.* **D23** (1981) 349; A.D. Linde, *Phys. Lett.* **108B** (1982) 389; A. Albrecht and P.J. Steinhardt, *Phys. Rev. Lett.* **48** (1982) 1220.
130. C.J. Copi and D.N. Schramm, astro-ph/9504026.
131. C.J. Copi, D.N. Schramm and M.S. Turner, astro-ph/9506094; S. Sarkar, Oxford preprint OUTP-95-16P (1995) and references therein.
132. D. Hegyi and K.A. Olive, *Ap. J.* **303** (1986) 56.
133. MACHO Collaboration, C. Alcock *et al.*, *Phys. Rev. Lett.* **74** (1995) 2867. EROS Collaboration, R. Ansari *et al.*, astro-ph/9511073.
134. J. Ellis and P. Sikivie, *Phys. Lett.* **B321** (1994) 390.
135. M. Rowan-Robinson, CERN Colloquium (1995).
136. J. Bardeen, P.J. Steinhardt and M.S. Turner, *Phys. Rev.* **D28** (1983) 679; A.H. Guth and S.-Y. Pi, *Phys. Rev. Lett.* **49** (1982) 1110; A.A. Starobinsky, *Phys. Lett.* **117B** (1982) 175; S.W. Hawking, *Phys. Lett.* **115B** (1982) 295.
137. J.P. Ostriker, *Ann. Rev. Astron. Astrophys.* **31** (1993) 689.
138. R. Brandenberger, *Current Trends in Astrofundamental Physics*, eds.

N. Sanchez and A. Zichichi (World Scientific, Singapore, 1993) p. 272.
139. M. White, D. Scott and J. Silk, *Ann. Rev. Astron. Astrophys.* **32** (1994) 319.
140. G. Smoot *et al.*, *Ap. J.* **360** (1990) 685.
141. R.K. Schaefer and Q. Shafi, *Nature* 359 (1992) 119; M. Davis, F.J. Summers and D. Schlegel, *Nature* **359** (1992) 393; A.N. Taylor and M. Rowan-Robinson, *Nature* **359** (1992) 396.
142. Ya.B. Zel'dovich, *Astron. Astrophys.* **5** (1970) 84; J.R. Bond, G. Efstathiou and J. Silk, *Phys. Rev. Lett.* **45** (1980) 1980.
143. J. Ellis, J.S. Hagelin, D.V. Nanopoulos, K.A. Olive and M. Srednicki, *Nucl. Phys.* **B238** (1984) 453.
144. P. Fayet, *Unification of the Fundamental Particle Interactions*, eds. S. Ferrara, J. Ellis and P. van Nieuwenhuizen (Plenum Press, N.Y., 1979) p. 587.
145. J. Rich, M. Spiro and J. Lloyd-Owen, *Phys. Rep.* **151** (1987) 239.
146. P. Renton, to appear in *Proceedings of the Beijing International Symposium on Lepton and Photon Interaction*, Oxford Preprint OUNP-95-20 (1995).
147. H. Goldberg, *Phys. Rev. Lett.* **50** (1983) 1419.
148. J. Ellis, G. Ridolfi and F. Zwirner, *Phys. Lett.* **B237** (1990) 423; L. Roszkowski, *Phys. Lett.* **B252** (1990) 471.
149. See, e.g., J. Ellis and L. Roszkowski, *Phys. Lett.* **B283** (1992) 252.
150. G. Jungman, M. Kamionkowski and K. Griest, Syracuse preprint SU-4240-605 (1995).
151. J. Silk and M. Srednicki, *Phys. Rev. Lett.* **53** (1984) 624.
152. R.L. Golden *et al.*, *Phys. Rev. Lett.* **43** (1979) 1196; M.H. Salamon *et al.*, *Ap. J* **349** (1990) 78; R.E. Streitmatter *et al.*, *Proc. 21st Int. Cosmic Ray Conf.* **3** (1990) 277.
153. R.J. Protheroe, *Ap. J.* **251** (1981) 387.
154. J. Ellis *et al.*, *Phys. Lett.* **B214** (1988) 403.
155. AMS Collaboration, V.M. Balebanov *et al.*, *An Antimatter Spectrometer to Search for Antimatter in Space on the International Space Station ALPHA* (1995).
156. L. Bergstrom, *Nucl. Phys.* **B325** (1989) 647.
157. J. Silk, K.A. Olive and M. Srednicki, *Nucl. Phys.* **279** (1987) 804.
158. A. Gould, *Ap. J* **321** (1987) 560.
159. J. Ellis, R.A. Flores and S. Ritz, *Phys. Lett.* **B198** (1987) 493.
160. F. Halzen, astro-ph/9508020.
161. M. Goodman and E. Witten, *Phys. Rev.* **D30** (1985) 3059.
162. J. Ellis and R.A. Flores, *Nucl. Phys.* **307** (1988) 883, **B400** (1993) 25

and *Phys. Lett.* **B263** (1991) 259.
163. K. Griest, *Phys. Rev.* **D38** (1988) 2357.
164. J. Engel and P. Vogel, *Phys. Rev.* **D40** (1989) 3132; A.F. Pacheco and D. Strottman, *Phys. Rev.* **D40** (1989) 2131; F. Iachello, L. Krauss and G. Maino, *Phys. Lett.* **B254** (1991) 220.
165. R. Peccei and H.R. Quinn, *Phys. Rev. lett.* **38** (1977) 1440 and *Phys. Rev.* **D16** (1977) 1791; S. Weinberg, *Phys. Rev. Lett.* **40** (1978) 223; F. Wilczek, *Phys. Rev. Lett.* **40** (1978) 279.
166. L. Abbott and P. Sikivie, *Phys. Lett.* **120B** (1983) 133; J. Preskill, M. Wise and F. Wilczek, *Phys. Lett.* **120B** (1983) 127; M. Dine and W. Fischler, *Phys. Lett.* **120B** (1983) 137.
167. R. Davis, *Phys. Rev.* **D32** (1985) 3172 and *Phys. Lett.* **180B** 225; D. Harari and P. Sikivie, *Phys. Lett.* **B195** (1987) 361; C. Hagmann and P. Sikivie, *Nucl. Phys.* **B363** (1991) 247.
168. F.T. Avignone *et al.*, *Phys. Rev.* **D35** (1987) 2752.
169. For a review, see G. Raffelt, *Phys. Rep.* **198** (1990) 1.
170. J. Ellis and K.A. Olive, *Phys. Lett.* **B193** (1987) 525; D.N. Schramm, *Comm. Nucl. and Part. Phys.* **A17** (1987) 239.
171. K. Hirata *et al.*, *Phys. Rev. Lett.* **58** (1987) 1490.
172. R.M. Bionta *et al.*, *Phys. Rev. Lett.* **58** (1987) 1494.
173. R. Mayle *et al.*, *Phys. Lett.* **B203** (1988) 188 and **B219** (1989) 515.
174. J. Ellis, D.N. Schramm, G. Sigl, M.S. Turner *et al.*, in preparation (1995).
175. P. Sikivie, *Phys. Rev. Lett.* **51** (1983) 1415; P. Sikivie *et al.*, Proposal to NSF for Research in Dark-Matter Axion Physics (1993).